CIRP Annals - Manufacturing Technology 60 (2011) 821–842

Contents lists available at ScienceDirect

CIRP Annals - Manufacturing Technology

journal homepage: http://ees.elsevier.com/cirp/default.asp

Computed tomography for dimensional metrology

J.P. Kruth (1)[a,*], M. Bartscher[b], S. Carmignato[c], R. Schmitt (2)[d], L. De Chiffre (1)[e], A. Weckenmann (1)[f]

[a] Katholieke Universiteit Leuven (K.U.Leuven), Department of Mechanical Engineering, Division PMA, Belgium
[b] Physikalisch-Technische Bundesanstalt (PTB), Braunschweig, Germany
[c] University of Padova, DTG, Department of Management and Engineering, Italy
[d] RWTH Aachen University, WZL, Chair of Metrology and Quality Management, Germany
[e] Technical University of Denmark (DTU), Department of Mechanical Engineering, Denmark
[f] University Erlangen-Nuremberg, Chair Quality Management and Manufacturing Metrology (QFM), Germany

ARTICLE INFO

Keywords:
Quality control
Metrology
X-ray computed tomography (CT)

ABSTRACT

The paper gives a survey of the upcoming use of X-ray computed tomography (CT) for dimensional quality control purposes: i.e. for traceable measurement of dimensions of technical (mechanical) components and for tolerance verification of such components. It describes the basic principles of CT metrology, putting emphasis on issues as accuracy, traceability to the unit of length (the meter) and measurement uncertainty. It provides a state of the art (anno 2011) and application examples, showing the aptitude of CT metrology to: (i) check internal dimensions that cannot be measured using traditional coordinate measuring machines and (ii) combine dimensional quality control with material quality control in one single quality inspection run.

© 2011 CIRP.

1. Introduction

Today X-ray computed tomography (CT) finds applications in three major fields. CT scanners for *medical imaging* go back to the early 1970s [1,49]: 1st scanner built by Nobel Prize winner Hounsfield in 1969 and 1st patient brain scan performed at the Atkinson Morley Hospital, Wimbledon, UK, in October 1971. Since 1980, CT became popular for *material analysis* and non-destructive testing (NDT) [70]: e.g. for observing the inner structure of materials (e.g. fiber-reinforced plastics) and detecting material defects. The cabinets of material testing CT devices are often small and aimed at hosting samples cut out from larger objects. More recently, CT technology entered the application field of dimensional metrology, as an alternative to tactile or optical 3D coordinate measuring machines, measuring arms, fringe projection systems, etc. (Fig. 1). The first attempts to perform dimensional measurement using existing CT scanners appeared around 1991 [10,19,64,99] but accuracy was not better than about 0.1 mm. An important breakthrough came in 2005, when the 1st dedicated dimensional CT machine [98] was exhibited at the Control Fair in Germany. From then on, several other machine vendors started offering larger and more powerful industrial CT devices able to host full workpieces and radiate through their large volume and/or mass [e.g. 32, 67, 98, 101, 103].

So far, dimensional CT metrology is the only technology able to measure as well the inner as the outer geometry of a component without need to cut it through and destroy it. As such, it is the only technology for industrial quality control of workpieces having non-accessible internal features (e.g. components produced by additive manufacturing) or multi-material components (e.g. 2K injection molded plastic parts or plastic parts with metallic inserts): Fig. 2a and b. The advent of those production methods favoring the trend for more part feature integration and yielding parts with complex internal geometries or multi-material components, is a major incentive that boosts the demand for dimensional CT metrology: industry can no longer accept that intricate components produced by additive manufacturing or multi-material injection molding escape any geometrical and tolerance quality control for the only reason that there is no non-destructive method to measure the inner or internal geometry. Dimensional CT metrology is also interesting for quality control of assemblies in assembled states, since the geometry and dimensions of components may differ in unassembled and assembled state: an assembly may fail geometrically, even if all individual elements of the assembly meet the tolerances when unassembled. CT being a non-contact measuring technique, it also might become a competitor to other novel non-contact quality inspection methods, like fringe projection, laser scanners, etc.

Another major advantage of industrial CT technology is that it allows performing dimensional quality control and material quality control simultaneously. In Fig. 2a CT measurement was not only used to check geometrical tolerances, but at the same time glass weld quality and porosity in bulb and socket have been checked. For further examples, see Figs. 12, 33 and 34.

Although the three fields of application (medical, material analysis, dimensional metrology) rest on the same physical and mathematical principles, the devices and procedures are quite different as they have to fulfill diverse requirements: see Fig. 1. In medical applications the doses of radiation and hence power have to be limited to protect the patient. The object (patient) cannot be rotated the same way as material samples or mechanical workpieces in technical CT scanners. Moreover, requirements on accuracy and spatial resolution are usually relatively low for

* Corresponding author.

0007-8506/$ – see front matter © 2011 CIRP.
doi:10.1016/j.cirp.2011.05.006

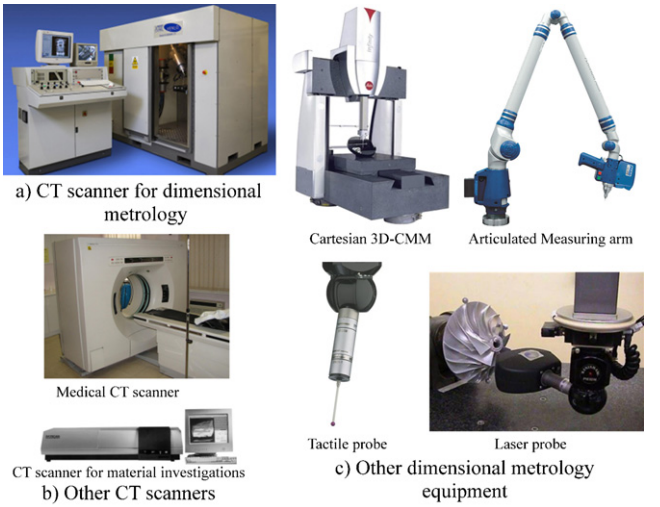

Fig. 1. Typical CT devices (medical, material, metrology) and dimensional measuring machines (CT, CMM, articulated arm).

medical scanners. Dimensional CT metrology lies at the other end of the specification scale: it often calls for high penetration power as there is a demand for measuring ever larger and thicker workpieces made of more absorbing materials (e.g. metals). Furthermore dimensional quality control requires high spatial resolution and *accuracy* in respect of the rules of measurement uncertainty [42,43] and traceability to the SI unit of measurement (the meter). Even though CT has been developed and applied in medical and material sciences for several decades, its application to dimensional metrology is therefore far from trivial and still requires substantial developments to bring it to maturity.

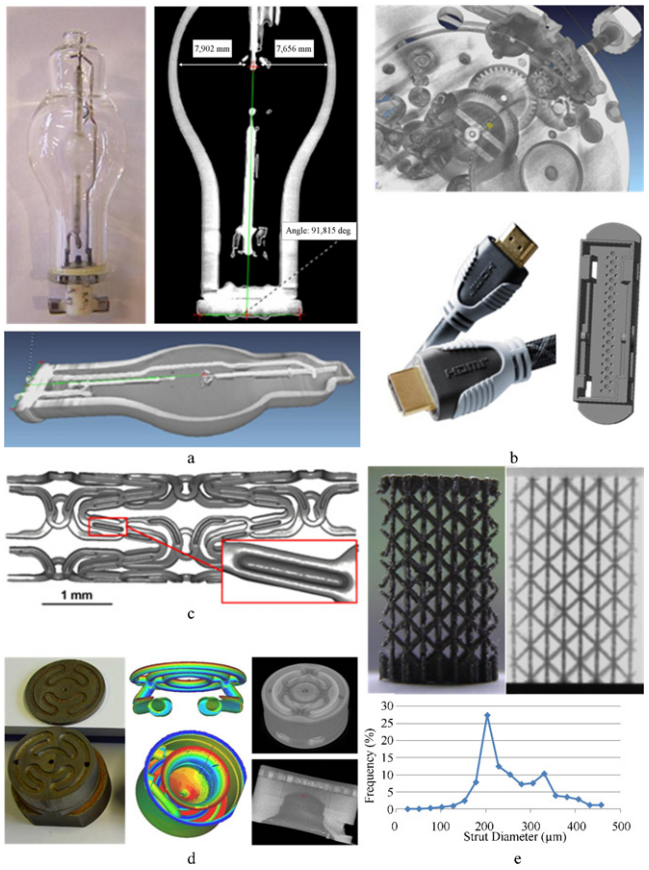

Fig. 2. Typical parts calling for CT metrology: (a) measuring squareness and electrode distance in multi-material lamp bulb; (b) multi-material assemblies/mechanisms (watch and connectors); (c) measuring drug eluting cavities in stent; (d) layered manufactured nozzle with complex internal channels; (e) measuring beam thickness in medical bone scaffold.

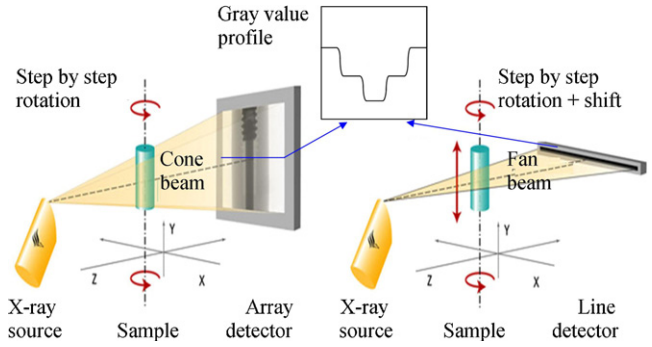

Fig. 3. 2D flat panel detector with cone beam and 1D line detector with fan beam (after [32]). A gray value profile along one pixel line is shown.

This paper summarizes the relevant general and specific principles of CT technology for dimensional metrology. It further gives the state of the art of dimensional CT metrology.

2. Basic principles

Fig. 3 illustrates the setup of a tomograph. A source generates X-rays. As the X-rays propagate through the workpiece material, the X-rays are attenuated due to absorption or scattering (see Section 5.3). The amount of attenuation is determined by the length traveled in the absorbing material, by the material composition and its density (i.e. attenuation coefficient μ) and by the energy of the X-rays. Measuring this attenuation allows to detect the presence of material (even of various materials in case of multi-material workpieces), as well as the lengths traveled inside the various materials: see 3D reconstruction in Section 3.2.1. The attenuation is measured by capturing the remaining X-rays that traverse the workpiece by means of an X-ray detector, resulting in a 2D gray image in case of a flat panel detector or a 1D gray profile in case of a 1D line detector. Images are taken from different angular positions of the workpiece. Mathematical reconstruction [48] of these projected images leads to a 3D voxel model (a voxel is the 3D analogue of a pixel), where the voxel gray value is a measure for the absorptivity of the material (i.e. composition, density, etc.). The next steps concern the post-processing of the voxel data, including the detection of the workpiece edges (segmentation) and subsequent dimensional measurement and quality control.

3. Technical systems and components

3.1. Hardware

3.1.1. X-ray sources

The X-ray tube (vacuum tube) typically consists of an electron beam gun containing a cathode filament emitting electrons, an anode accelerating the electrons, a Wehnelt grid electrode for control of the electron beam (convergence and intensity of beam) and magnetic deflectors and lenses to focus the electron beam onto a target that will generate X-rays (Fig. 4). When hitting the target, the fast electrons are decelerated very suddenly, causing their energy to be converted into heat (over 99%) and X-rays (less than 1%). Having a small electron beam or X-ray spot is essential to obtain sharp images (Fig. 8). Nanofocus spots of less than or around 1 µm diameter are achievable with X-ray photon energies up to 250 keV, being defined as the energy of an electron when accelerated by an applied voltage of 250 kV. For voltages above 250 kV, the heat dissipated at the target gets that large that it may no longer be concentrated in a micrometer spot: such tubes are then called micro-focus sources with spot diameters ranging typically from 30 to 1000 µm. Today X-ray tube voltages are limited to 450 kV for commercial standard tubes, while 800 kV specimens are under test. At the exit of the X-ray tube, the X-ray

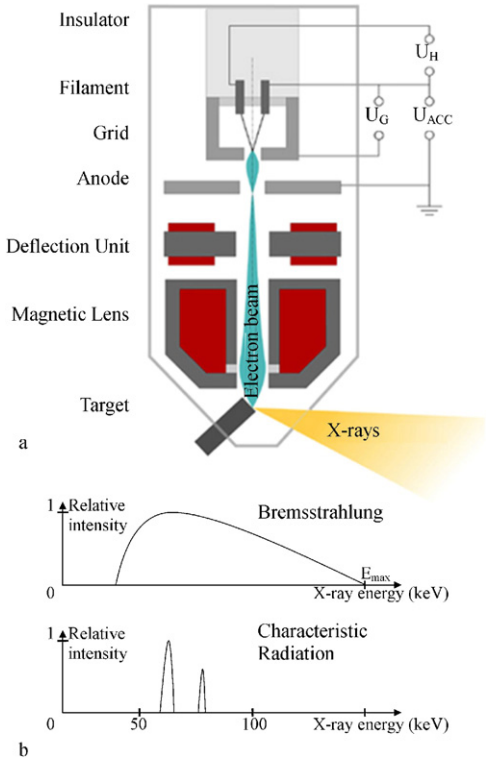

Fig. 4. Typical X-ray tube [67] and radiation spectra.

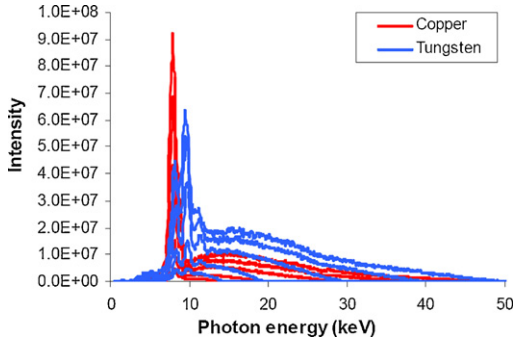

Fig. 5. Spectra of Cu and W targets from 15 to 50 kV applied voltage in steps of 10 kV [52,53]. Spectra measured with a Tomahawk source at K.U.Leuven-MTM in cooperation with the University of Sassari, Italy.

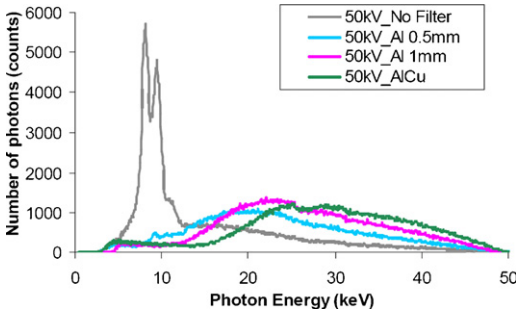

Fig. 6. Spectra for 50 kV source before and after passing various filters (larger count time when using filters) [52,53].

beam is generally "shaped" by passing through a circular aperture or diaphragm (for conical beams) or through collimating plates (flat fan beam, see Fig. 7) and through a beryllium window sealing the vacuum source.

The target can be made from different materials, depicting different X-ray radiation spectra. It may be a transmitting target (thin plate) or a reflective target (massive target as shown in Fig. 4). Thin transmitting targets are only used for low power CT sources, as they cannot resist high temperatures. High power CT sources are therefore generally equipped with water cooled massive reflective targets. In some cases high precision rotating targets are used to spread the heat input over a larger area. In "open tubes", the operator may himself change targets if worn or burned, or to change target material (radiation spectra). Some sources have multi-material targets, where different target materials are fitted on an indexable head, in order to allow easy multi-spectra measurement (e.g. for multi-material objects and for achieving better resolution and image quality for lower absorbing materials as plastics).

The produced X-ray radiation consists of "Bremsstrahlung radiation" and "characteristic radiation". Bremsstrahlung is the dominant X-ray production process. It takes place when an electron hits an atomic nucleus in the target, resulting in a sudden deceleration of the electron (hence the German term "Bremsstrahlung" or "braking radiation") and in emission of an X-ray photon. Bremsstrahlung yields a continuous X-ray spectrum from very low energies up to the full energy (i.e. applied keV) of the impacting electron (Fig. 4). Characteristic radiation occurs when a high energy electron impacts and excites an inner shell electron in an atom of the target. De-excitation of that or a substituting electron (in case the inner shell electron is ejected and the vacancy is filled by an electron of a higher energy level) yields release of the electron's energy and of a photon of characteristic radiation. It is called "characteristic" because the energy of the radiation depends upon the target material and is characterized by a line spectrum, see Fig. 4 [2]. Fig. 5 shows the total emission spectrum of a tungsten and a copper target at 15–50 kV source voltage (compare to Fig. 6 and to Fig. 19 for high kV source).

The generated X-ray radiation is characterized by its energy distribution (also called quality) and its intensity (flux). The highest X-ray energy present in the X-ray spectrum determines the penetrating power of the X-ray beam into matter. The intensity of an X-ray beam is a measure of the amount of radiation energy flowing per unit of time [2].

Besides the common X-ray sources based on an *electron gun* (Fig. 4), more expensive *linear accelerator* (LINAC) X-ray sources are used for industrial NDT or dimensional CT measurements of larger and high absorbing parts (e.g. meter thick blocks of concrete or steel). Today, large *synchrotron* radiation facilities are also used to generate X-rays for CT applications, including research for dimensional measurements [18,21,69]. Synchrotron CT devices are present as permanent installations or as user accessories at nearly all synchrotron facilities (e.g. ESRF, HASYLAB/DESY). Synchrotron radiation offers unique X-ray beam properties. The source itself offers a broad band of X-ray energies with a very high flux (intensity) and a high brilliance. The latter is due to the low angular dispersion of the beam. Such a quasi parallel beam eliminates common problems associated to cone or fan beams and image magnification, thereby improving edge detection and measurement accuracy. Synchrotron X-ray beamlines are often provided with monochromators producing a beam with a very narrow energy distribution and a tunable energy. Monochromatic X-ray beams are a remedy to the problems of "beam hardening" typical to wide beam spectra (see Section 6.1). Even when monochromatized, synchrotron X-ray beams offer a higher intensity compared to classical X-ray tubes. Synchrotron X-rays are available in quasi continuous mode: times for the refill of the storage rings are in orders of many hours allowing measurement times of the same order. In some cases synchrotron CT measurements, especially when using monochromators, need to be corrected for a time varying intrinsic pattern visible in the flat field of the radiation.

3.1.2. X-ray detectors

The CT detectors used nowadays are either flat panel detectors consisting of a 2D array of pixels, or straight or curved line detectors consisting of a 1D array of pixels (Fig. 3).

1D line detectors yield a higher accuracy, are more efficient and resist higher X-ray energies allowing thicker objects to be measured. However, the use of a line detector is more time

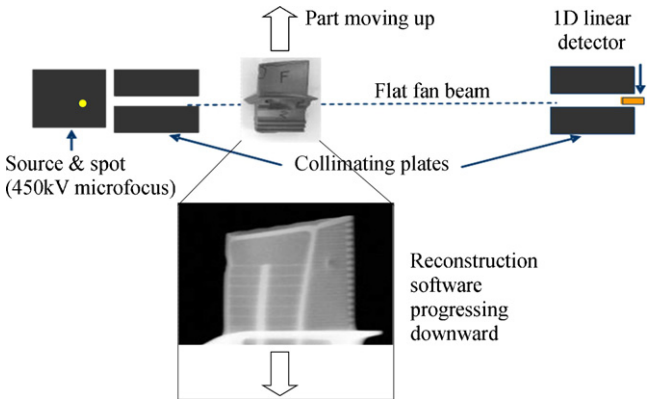

Fig. 7. Linear detector with collimated beam [7].

consuming as only one slice is measured during one rotation of the workpiece and as the object should be displaced in the *Y*-direction for every new slice to be measured. Measuring a workpiece of 100 mm height with an interslice distance of 100 μm results in 1000 slices and a measuring time that might be 1000 times larger than with a 2D detector. The higher accuracy results from the fact that line detectors allow to use collimated X-ray beams (fan beam rather than cone beam) and yield less pixel interaction or scatter (no adjacent pixels in *Y*-direction, thin shielding plates separating pixels in the *X*-direction, collimating plates in *Y*-direction below and above detector pixel array): Fig. 7. 1D detectors usually feature thicker scintillators than flat panel detectors. Thus, they can detect a higher percentage of the incident X-ray and offer therefore – for a fixed X-ray energy and exposure time – a better signal-to-noise or S/N ratio than flat panel detectors. Additionally, 1D detectors can be curved rather than straight, with the arc center coinciding with the X-ray spot, thereby reducing deformation of the image when moving away from the central pixel.

Basically, there are three detector principles. Either the output of the detector is proportional to the total number of photon impacts (counting-type detectors), or it is proportional to the total photon energy (scintillation-type detectors or 'indirect' detectors), or it responds to energy deposition per unit mass (ionization detectors) [48]. The most successful and widely used detectors are 'indirect' ones. They are often based on amorphous silicon TFT/photodiode arrays positioned behind X-ray scintillators that convert the X-rays into visible light [13].

Nowadays, standard commercial 2D detectors have a maximum resolution of 2048 × 2048 pixels at a pixel size of 200 μm and commonly withstand powers up to about 250 keV (although high power panels are showing up). At high power (80 keV to 10 MeV), 1D detectors are commonly used, which may include over 3000 pixels at 250 μm pitch.

3.1.3. Kinematic systems

In a medical CT scanner, the X-ray tube(s) and the detector continuously rotate around the measured object (patient), while the object is translated horizontally through the space between tube and detector. In a metrological CT scanner, the X-ray tube and detector are usually fixed, while the object rotates in the space between tube and detector, either without translation movement (when using a 2D detector) or with a vertical translation (1D detector). The basic axes configuration of industrial CT scanners is given in Fig. 3.

The basic kinematic system usually consists of:

1 A turntable for stepwise or continuous rotation of the workpiece.
2 A horizontal translation axis for positioning the turntable with the workpiece between the X-ray source and the detector (*Z*-direction). This axis is often referred to as the magnification axis: higher geometrical magnification is achieved by positioning the object closer to the source (Fig. 8). Higher magnification however yields a positive and negative effect: it increases the image resolution, but it also causes more blurred images, due to the finite X-ray spot size.
3 Optionally: a horizontal translation axis in *X*-direction to move the turntable (and workpiece) parallel to the detector. This translation axis enables positioning the workpiece in and outside the field of measurement, e.g. for placing the turntable subsequently in different horizontal positions in rotate-translate-type scanning or rotation-only offset scanning for large magnification or large objects, or for the stitching of projections for larger parts when using a rotation mode.
4 A vertical translation axis moving turntable and workpiece (or source and detector). When using 2D flat panels, this axis is used for positioning the workpiece (or a specific region of interest in case of tall workpieces) in the measuring field (detector) and/or for the stitching of measuring regions of a larger vertical part that has to be measured in several times. For CT systems with 1D detectors, the vertical axis provides the necessary stepwise translation for slice scanning or continuous translation for spiral CT.

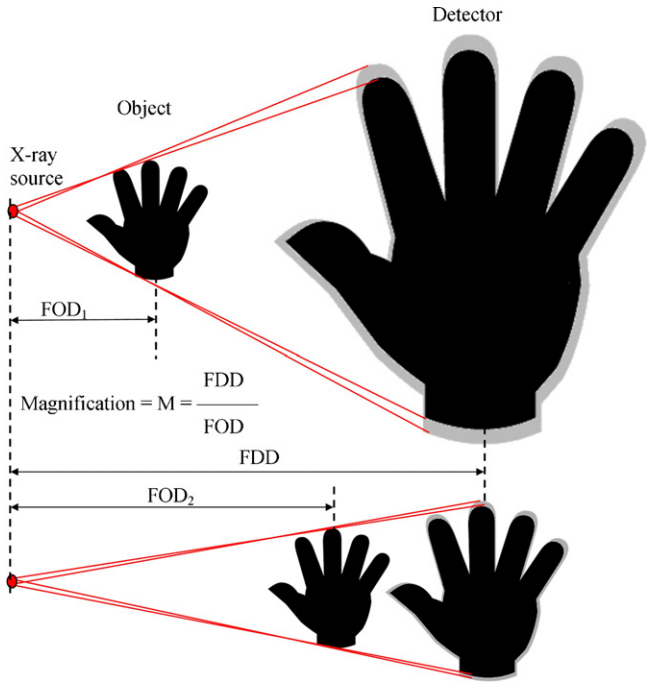

Fig. 8. Image magnification and blurring by moving the object towards the source having a finite X-ray spot.

The machine components should have high accuracy and stability (geometrical and thermal) as they affect measurement outcome: positioning errors of the turntable and its quality of rotation affect the quality of reconstruction; positioning errors and repeatability of the *Z*-axis directly influence the measured dimensions through a change in magnification factor (Fig. 11).

Extra translation axes may be added for both source and detector, in order to meet specific requirements and increase machine flexibility, e.g. for stitching procedures, dedicated scanning strategies or error compensation techniques.

3.2. Software

3.2.1. CT specific software: reconstruction and edge detection

Apart from the CT hardware, software plays a vital role, especially for the reconstruction of the volume model out of the acquired 2D projection images. Reconstruction is usually done by "*filtered back-projection*", which is based on the "Linear Integral Transformation", a mathematical model developed by J. Radon in 1917. The model describes the absorption of X-rays when passing

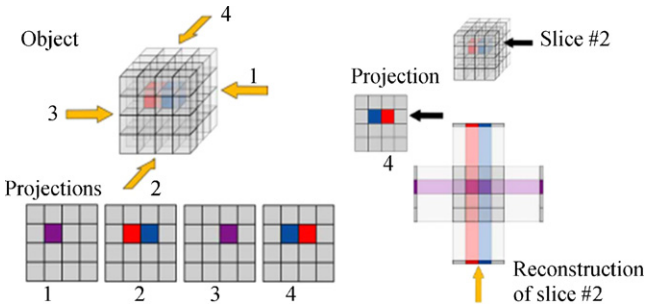

Fig. 9. Example of back-projection reconstruction.

through a medium with varying linear attenuation coefficient μ:

$$I = I_o \exp\left[-\int \mu(x)\,dx\right] \quad (1)$$

which goes back to the Beer–Lambert law expressing the exponential attenuation of electromagnetic radiation with initial intensity I_0 traveling a distance x in an absorbing medium μ:

$$I(x) = I_o\, e^{-\mu x} \quad (2)$$

In CT, μ also varies with X-ray photon energy E in accordance to the absorption spectrum of the material (Fig. 17) [68].

The input for the reconstruction are the "gray value profiles" (see Fig. 3) representing the evolution of the intensity along the pixels located on one line of the detector, i.e. pixels lying in a *XZ* section of the object (be it a linear detector or a flat panel detector). Fig. 9 illustrates the principle of back-projection for an object having two voxels with different attenuation μ. The remainder of the "reconstruction volume" (here a cube of $4 \times 4 \times 4$ voxels) is filled with air, i.e. no material. The reconstruction example is based on 4 projections taken at 0°, 90°, 180° and 270°.

When using a cone beam source, the reconstruction should account for the fact that voxels do not stay in the same horizontal projection plane while the part rotates. The reconstruction is then based on the Feldkamp algorithm [29]. This reconstruction is very sensitive to horizontal misalignment of the source, rotation axis and detector. It requires regular calibration (e.g. using a high absorbing tungsten wire) and adequate error correction (see Section 6.2).

Fig. 10 shows the result of the reconstruction when scanning three aligned balls using an increasing number of angular poses (from 4 to 128). With 4 angular poses the reconstruction is very vague and resembles more as if a grid of 3×3 square objects has been measured. As the number of poses augments, the reconstruction becomes more precise, ending with an accurate picture of the three balls.

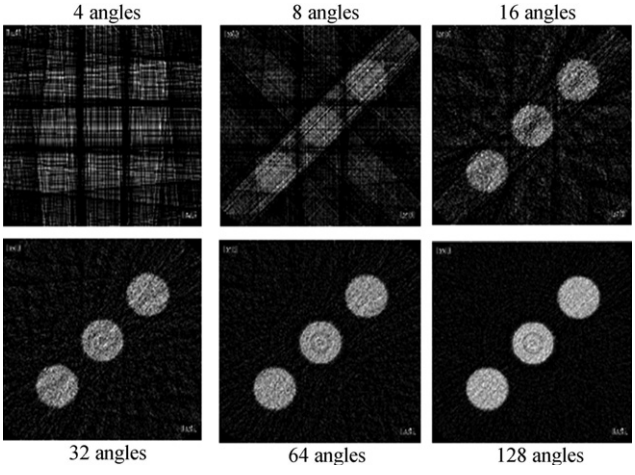

Fig. 10. More angular poses improve reconstruction accuracy, but enlarge measurement time.

This explanation clarifies that the resolution of the measurement and reconstruction is influenced by pixels size, number of pixels within each gray value profile (i.e. number of detector pixels in *X*-direction), number of detector pixels or slices in the *Y*-direction (not necessarily equal to the number of pixels in the *Y*-direction for a flat panel detector), number of angular positions (poses) at which images are taken, number of projection images taken in one angular pose (averaging number), binning (i.e. combination of adjacent pixels), etc.

The 3D reconstruction is followed by the *edge (surface) detection or segmentation* determining the respective interfaces between solid materials and surrounding air or between different solid materials. The edge detection converts 3D voxel data into 3D surface data. Various techniques exist to identify object or material edges: assigning a threshold gray value to "edge voxels", interpolation between voxel gray values, search for maximum gray value derivatives, mid gray value between light air voxel and dark material voxel levels, local adaptive gray threshold, etc. (see Section 7.4, Fig. 23). The threshold method greatly influences the resolution (sub-pixel resolution), as explained in Sections 7.2–7.4. Beam hardening and other image errors/artifacts (Section 6) may disturb correct edge detection, as it alters the gray value of edge pixels.

The influence of the reconstruction software on the measuring accuracy is further elaborated in the next sections.

3.2.2. Dimensional analysis software

While 3D reconstruction software is used in all CT systems, CT systems for dimensional metrology call for additional specific software to extract geometrical features (like planes, cylinders, spheres, etc.) and calculate geometrical data (position, orientation, dimension, length, diameter, angle, form errors, measurement uncertainty, etc.). Dimensional analysis often requires different data processing steps: conversion to point cloud, facetted surface models, geometric features or CAD model on which dimensional measurements can be performed. This requires special data conversion and analysis software and different processing steps that will be detailed in Section 4.2. The software should support most dimensional measuring tasks available in traditional CMM software packages.

4. Workflow for dimensional metrology

Applying CT for dimensional measurements involves several steps, some being common to other CT applications, others being very specific for dimensional measurement.

The two first steps are related to the physical measurement (i.e. it involves the measuring hardware), where the other steps are post-measurement data processing steps.

4.1. Steps related to the measuring hardware:

- *Scale identification (also called "scale calibration").* Performing precise and traceable dimensional measurements requires calibration of the size of the 'image pixels' and 'model voxels'. This "calibration" is mostly done by measuring a simple calibrated reference object (two spheres on a bar or plate, a gauge block or stepped pyramid with well known dimensions; see Section 7.3). This measurement can be done prior, together or/and after the measurement of the actual workpiece. This measurement allows identifying a global scale factor to link the pixel or voxel size to the unit of length (meter/micrometer). It is important to do this calibration for a position of the magnification axis (position of rotary axis, see Fig. 8) that coincides with the position that will be used during the actual measurement, since lack of repeatability in axis positioning may change the scale factor and introduce relative errors of the order of 1.5×10^{-3}: see Fig. 11 showing the scale factor variation over

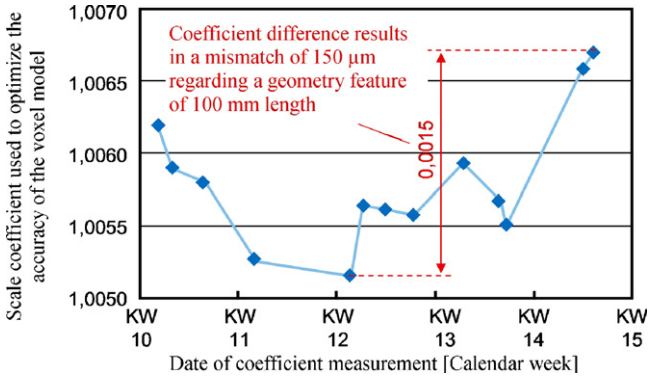

Fig. 11. Temporal scale coefficient variation.

a period of five weeks. It might be necessary to identify different pixel or voxel sizes (scales) in the *X*- or *XZ*- and the *Y*-directions, because pixel sizes of a flat panel detector may differ in *X* and *Y*, or because a different scale applies to pixels of the line detector (*X*-direction) and the *Y* movement of the *Y*-axis. Basically, the scale factor will also differ along a pixel line of the detector from the central pixel to the most outward pixels. A raw and initial calibration of the scale factor and image pixel size depending on the pixel's *X* and *Y* position is normally done when the detector is installed and has only to be redone at large time intervals. However, precise voxel calibration has to be redone almost for each single measurement, as it changes among others with the applied magnification. Common procedures for voxel size calibration are explained in Section 7.3. Commonly used calibration objects are described in Section 7.7.

- *X-ray part measurement*. As will be explained in Section 5, a lot of parameters affecting the X-ray imaging process have to be selected when starting measurements: source current, source voltage, type of target (material, shape, etc.), magnification, number of angular poses, exposure time, number of projection images per pose (image averaging), sensitivity of the detector, binning, waiting time after turntable movement, number of positions along the *Y*-axis (number of slices for 1D detectors), use of filter plate (material, thickness, position), CT strategy (measuring the whole object at once or in parts), combining measurements with different current/voltages/targets, etc. Also the part orientation influences the amount of measuring noise and scatter (avoid horizontal planes yielding noise) and the material thickness that has to be penetrated (avoid pixel saturation or extinction). The adjustment of those parameters may require test measurements and iterative procedures. Up to now the parameter set-up and the part alignment are usually done by the system operator meaning a significant user influence. A lot of effort is devoted in trying to establish new procedures to select those parameters (e.g. databases, simulation software, knowledge based systems, etc.), without need for trial or iterative measurements [46,77]. Recently, expert systems are being developed [38,71,72] covering the choice of CT parameters and positioning of the part to be measured. First CT assistance products may be expected in some time, but true performance has to be proven for real complex parts and real measurement tasks: see Sections 5.2 and 5.3.

4.2. Subsequent data processing processes

The acquired gray images have to be processed in several steps to obtain dimensional measurand values and deviations (possibly linked to a measurement uncertainty and a go/nogo check against tolerances). Those steps are often carried out with different software packages: the first steps are often done with software provided by the CT machine builder, the next steps often use dedicated CT software from independent 3rd party software suppliers, while the last steps may be done using general purpose software for dimensional metrology (software used with conventional tactile or optical coordinate measuring machines, DMIS based software, CAD linked software, etc.).

- *X-ray projection raw data pre-processing*. This includes e.g. data shaping done by the detector firmware and bad pixel correction and linearization of the signal due to the energy dependant absorption of X-rays (beam hardening correction). In some cases the raw data are corrected geometrically. For raw data with lower S/N ratio or data suspected to show local deviations or blurness, median or Gaussian filtering may be applied locally.
- *3D voxel reconstruction from X-ray images*. This step has been explained in Section 3.2.1. This step might also include software corrections for beam hardening (Section 6). Some softwares offer half a dozen beam hardening algorithms or smoothing/filtering procedures. Many vendors offer different reconstruction schemes having e.g. different reconstruction kernels. Selecting the proper algorithm is often a matter of iteration and trial-and-error re-processing of pre-processed 2D images with other algorithms.
- *Rescaling, thresholding, edge detection, voxel interpolation*. This step too has been introduced in Section 3.2.1 and will be discussed later in Sections 7.2–7.4.
- *Conversion from voxel to surface/geometric model (STL model)*. The edge detection generally results in a point cloud (i.e. a collection of points located at the interface between various materials). This point cloud is then generally turned into a geometrical surface model by topological association of neighboring points. This association is generally done by generating a triangular mesh model that represents an open or closed facetted surface model of the scanned object and its different material regions. This facetted surface model is often formatted according to the STL format (Standard Triangulation Language) that was initially developed for Rapid Prototyping applications, but is now commonly used in other engineering applications like CAE, CAD or CAM. Other CAE or CAD data formats are also frequently supported.
- *Point, feature and coordinate extraction*. While point clouds and triangulated surface models might often be sufficient for visual rendering and basic volume calculations (e.g. void or porosity assessment) in medical and material applications, they are not suited for dimensional metrology applications. The latter requires precise identification of "measuring points" and coordinates that represent the measurand (i.e. dimension to be measured) or the feature to be assessed (e.g. location of apex and axis of a cone). Those points and coordinates generally do not coincide with data available in the CT point cloud generated in previous steps. Moreover, there is no association of points with certain geometrical part features (e.g. a planar, circular or cylindrical feature of the object) and the CT points are often not located as needed for dimensional measurement (e.g. not located in a single plane, not distributed as needed, not related or projected within the proper reference plane, etc.). Either the points should be automatically or interactively converted to features (planes, circles, cylinders, spheres, free-form surfaces, roughness profiles, etc.) that can be used in conventional CMM software for size or position identification (e.g. calculating a hole diameter or the distance or parallelism of a hole to a surface). Alternatively, the point clouds can be used as such within a point-cloud-based CMM software, as the softwares available for dimensional measurement using point clouds originating for laser scanners or photogrammetry measuring devices.
- *CMM software for measurand assessment*. Whether using point clouds or reconstructed geometric features, a dedicated CMM software is required to perform GPS assessments of form, position and size of part measurands and tolerances (GPS = Geometric Product Specification). Such software should cover all common procedures for dimensional metrology such as: identification of reference datum and local workpiece coordinate systems (according to a few tens of possible alignment

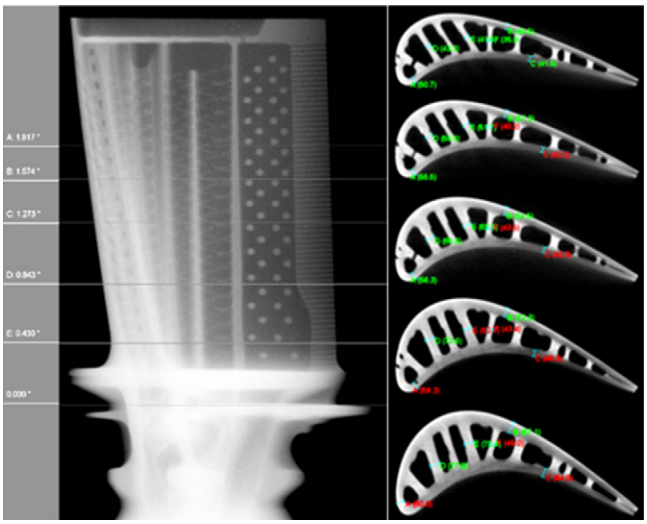

Fig. 12. Dimensional CT measurement on turbine blade (Courtesy Nikon-Metrology/X-Tek).

procedures), intra or inter-feature measurements (e.g. feature size or inter-feature distance or location, taking standardized measurand definition into account if standards exist), feature fitting algorithms (e.g. least square, maximum inscribed, minimum circumscribed, minimum deviation circles and cylinders), checking versus given tolerances, uncertainty calculation, etc. This should be done in application of the hundreds of existing standards on GPS and CMM measurements. Many procedures however are still not well defined or standardized. The step from point clouds to measurand assessment in CT metrology remains one of the critical steps in ensuring proper, accurate and traceable CT measurements. Examples of such CMM feature assessment are given in Figs. 12–14. In most cases, the CMM software should also allow combining various CT measurements and merge them with other tactile or optical measurements: see also Section 7.6 and [92]. This addresses the problem of alignment of various data sets (using reference datum or least square fit) and the use of one data set (e.g. few tactile measurements) to adjust the scale factors and edge detection threshold of CT measurements: see Section 7 and [54].

- *CAD comparison*. An actual-to-nominal comparison is often performed for analyzing the deviation of measured complex parts to a nominal CAD representation: see Figs. 14b and c and 33b. It is worthwhile to notice that this comparison is sensitive to the sequence of file, i.e. sensitive to which data set is set as nominal and which is set as actual. Depending on the geometry of the part the difference between a reversed analysis is not just a reversed sign but can have significant differences in the magnitude of deviations (esp. in areas of higher deviation and higher local curvature). Actual-to-nominal value comparisons are also performed analyzing different measured data sets, e.g. for analyzing deviations to a measured master part.
- *Dedicated feature analysis*. There exists dedicated feature analysis software to solve special customer requests. Frequently used analyses are wall thickness and porosity analyses which are typical for cast or molded parts. An example is given in Fig. 33. Further analysis tools aim e.g. at recognizing delamination or fiber orientation in carbon fiber reinforced plastics. Analysis modules exist as stand-alone software or are part of voxel based 3D analysis and visualization software.

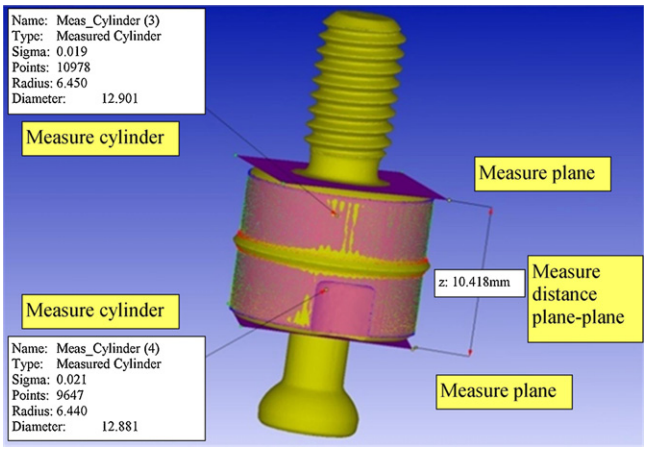

Fig. 13. Example of dimensional CT measurements.

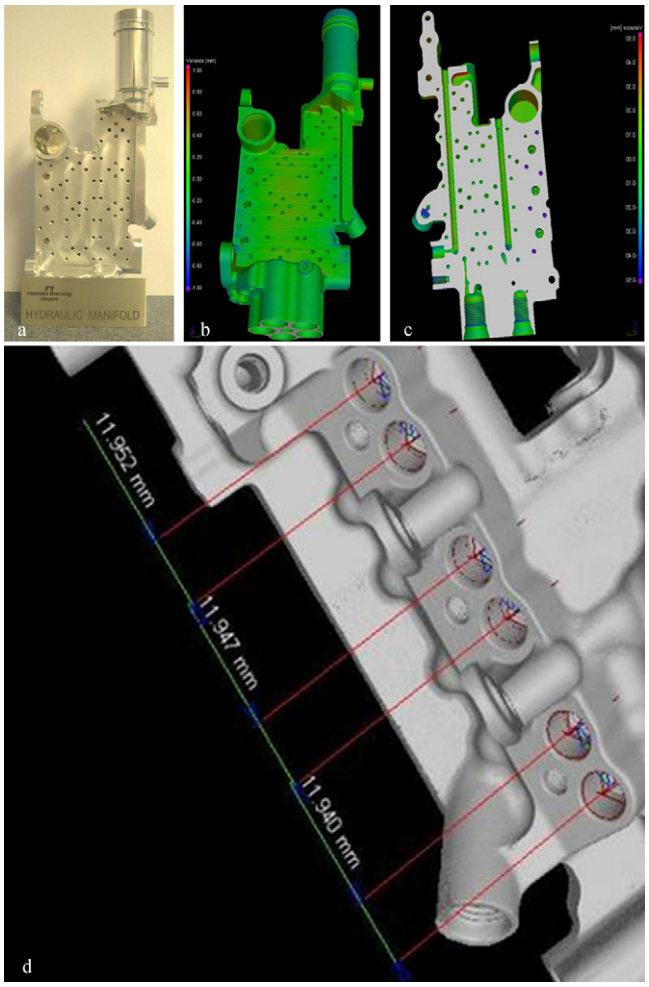

Fig. 14. CT control of individual dimensions (below) and comparison of outer and inner geometry with CAD model (above) [67].

5. Parameters and influencing factors

This section describes some parameters and factors influencing CT measurements that can be chosen or influenced by the operator to obtain proper CT images. Those parameters include: target, source power (voltage and current), workpiece orientation, scanning strategy, etc. Other parameters allowing to remedy imperfections of CT images (like beam hardening, scatter or noise) will be discussed in Section 6. Some of the latter parameters may also be chosen by the operator, e.g. choosing hardware beam filtering plates or specific numerical filtering for the reconstruction algorithms.

5.1. Target

The target of the X-ray source is characterized by its type (transmissive, reflective, rotating, etc.) and material (tungsten, rhenium, copper, molybdenum, etc.). Different materials mean

different proton numbers. The interactions of the filament emitted electrons with the atoms of the target material were explained in Section 3.1.1. They are obviously related to the proton number of the target material, which affects the radiation spectrum in various ways. It influences the intensity (i.e. amount of radiation - higher proton number increases the intensity) of the "Bremsstrahlung" and "characteristic radiation", and also the quality (i.e. penetrating power) of the radiation [2]. The target material should be selected to suit the required operation conditions: see also Section 5.3 (workpiece material). Some CT vendors offer facetted multi-material targets that can be indexed to sequentially measure with different spectra. Transmissive targets allow a nice circular X-ray emitting spot (X-rays are emitted in the same direction as impacting electrons and the X-ray spot exactly matches the electron beam spot, while the spot becomes elliptic and more scattered in oblique reflecting targets [35]). Transmissive targets however cannot support high energy densities. High power CT calls for water cooled reflective targets. Rotating reflection targets allow increasing the electron flux without damaging the target. Some CT devices are equipped with dual X-ray tubes or heads with different targets, or nano and micro focus sources.

5.2. Beam power

The power of an X-ray beam is characterized by the current and voltage applied to the electron beam that hits the target and generates X-rays. The current (μA) equals the rate of charge carriers (i.e. electrons) flowing from the source filament to the target. It directly influences the X-ray intensity (quantity or amount of radiation energy), but does not affect the beam quality (i.e. penetration power). Fig. 15a shows that doubling the current doubles the intensity across all photon energies of the spectrum [13]. The voltage (kV) affects both, energy distribution (maximum keV, quality, penetration) and intensity (amount of X-rays). It affects quality because the voltage determines the maximum photon energy and hence the penetration power. Fig. 15b shows the effects of doubling the voltage.

The choice of the proper voltage and current (and filter, see Section 6.1 on beam hardening) for a specific measurement is a difficult task. The voltage greatly changes the X-ray spectrum by extending it up to the kV voltage setting (keV units), hence including new specific radiation peaks in the spectrum: compare Fig. 6 and Fig. 19. The settings have to consider the part's material, density, geometry, etc. Part shape, size and material composition may vary substantially in dimensional CT metrology (unlike in CT analysis of material samples or in medical imaging). This often leads to contradicting boundary conditions: the voltage should on the one hand be set high enough to avoid total beam extinction in the direction where the largest amount of material has to be penetrated, but may on the other hand not lead to loss of contrast or saturation of the detector in the direction where less material is present. This might be a problem when measuring parts that are thick in one direction and thin in other directions or having elongated external or internal features, or when measuring multi-material parts. A way out, is to perform CT measurements at different current or power settings and to eliminate saturated or extinguished pixels before merging the gray values obtained at different power settings (after proper rescaling of the gray values): see Sections 7.5–7.6 [56]. Several researchers developed simulation software for determining proper power settings

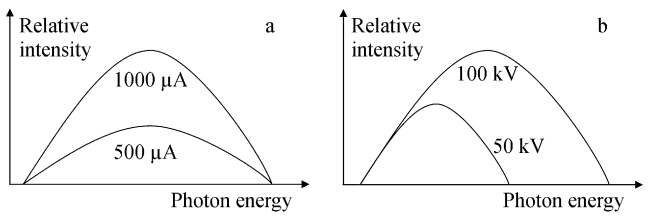

Fig. 15. Influence of source current and voltage.

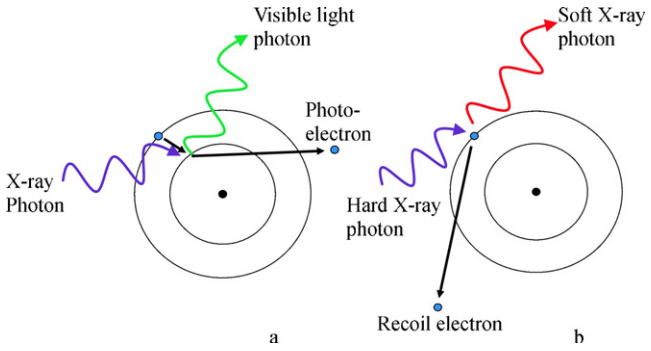

Fig. 16. Photoelectric absorption (a) and Compton scattering (b).

[53,63,88,102] but those simulators are often not suited to account for complex part geometries as encountered in dimensional measurements and do not account for all influence factors. Moreover, those simulators assume the spectrum of the source to be known, which is seldom the case (unless the spectrum is measured) since even sources with the same target material and power may have different spectra [84]. Available simulation software usually does not contain a quantitative treatment of scattering effects (scattering of X-ray photons with the workpiece and detector internal scattering) which is relevant for higher X-ray energies (e.g. greater than 250 keV). Hence, time-consuming experimental investigations of the optimal parameter settings can often not be totally excluded.

Multi-target measurements may be an alternative to multi-power measurement, but are more complex.

5.3. Workpiece material and geometry

The way X-rays are attenuated when passing through matter highly depends on the material and its attenuation coefficient μ (see Eq. (1)). The attenuation in the power range 20–450 kV (typical for industrial CT) is due to photoelectric absorption and Compton scattering: see Fig. 16. *Photoelectric absorption* occurs when the total energy of an incoming X-ray photon is transferred to an inner electron, causing the electron to be ejected. In *Compton (inelastic) scattering*, the incoming X-ray photon interacts with a free or outer electron, ejecting the electron. As a result of this interaction, the X-ray photon is deflected in a different direction with some loss of energy, which is gained by the electron. Both effects are energy dependent, but this dependence is larger for photoelectric absorption. The probability of a photon being lost from the original beam is thus function of its energy: i.e. the attenuation coefficient μ not only depends on the material composition and density, but is a strong function of X-ray energy (Fig. 17), while the beam is usually not mono-energetic (Fig. 6). The total attenuation, calculated by Eq. (1), is therefore the result of the initial X-ray spectrum emitted by the source $I_0(E)$ and the ray

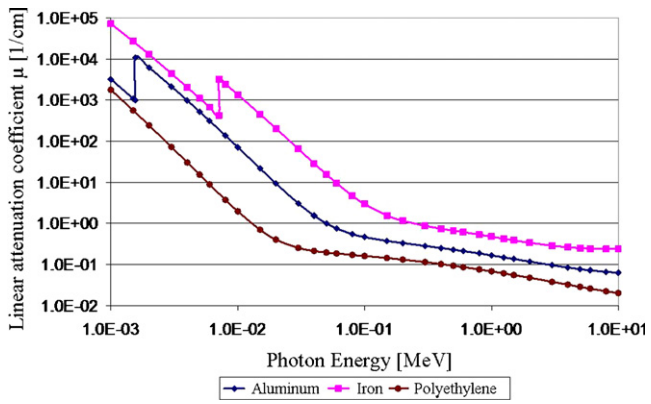

Fig. 17. Linear attenuation coefficient for different photon energies.

energy dependent linear attenuation coefficient of the material $\mu(E)$, summed up over the energy intervals ΔE and the length increments Δx traveled through solid material. A proper combination between emitted spectrum (target material) and absorption spectrum (workpiece materials) can largely influence the quality of the CT images and thus the measurement. In case of multi-material workpieces, multi-target measurements could offer benefits (Section 5.1). An alternative for measuring multi-material objects with different spectra is to vary the source power, as this also influences the spectrum (Section 5.2). Varying beam intensity (source current) does not affect the spectrum, but can help to achieve a better signal-to-noise ratio.

The material attenuation coefficient obviously limits the maximum accumulated material thickness that can be penetrated and hence limits the workpiece mass and maximum length. Typical values are given in Fig. 18. Skilled operators try to find an optimal part orientation minimizing the maximum penetrated material thickness or the variation of penetration depth when rotating the part (as to avoid saturation or extinguishment of pixels during capture of the X-ray images). Optimal part orientation should also avoid part surfaces perpendicular to the rotation axis (i.e. parallel to the X-ray beam), as this favors beam scattering and yields instabilities in 3D reconstruction (partial volume effects, tangent intersection, etc.). Beam scattering also varies with the X-ray photon energy. Tabulated or graphical values for attenuation (e.g. Fig. 17) and scatter versus photon energy can be found in literature [24] and on many websites [68].

5.4. Temperature control

One important difference between CT analysis for medical, material and dimensional applications is that the former two applications have no concern about temperature control for measuring at 20 °C. It is even generally not possible to bring living creatures or material to 20 °C. Dimensional metrology requires measurements to be at 20 °C and deviation from this standard temperature is often a major source of errors [15].

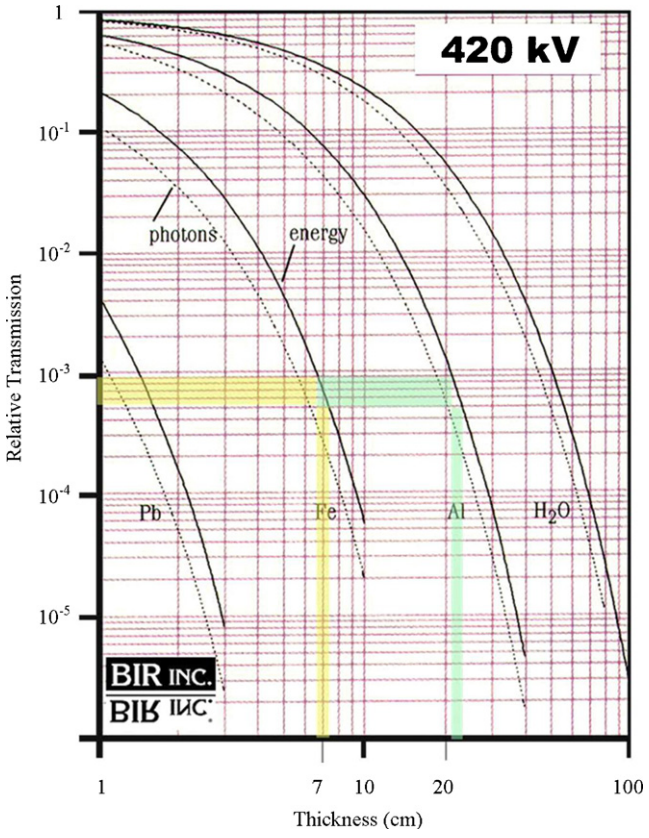

Fig. 18. Typical maximum penetrable material thicknesses.

Temperature control in dimensional CT is more cumbersome than with other length or coordinate measuring devices, because an industrial CT contains at least one large heat source within its enclosure, i.e. the X-ray source, but also motors, drives, detector and electronics might be disturbing heat sources. Traceable measurements are only possible if all elements (i.e. measuring scales, detector, structure separating source/workpiece/detector, workpiece itself, etc.) are at a uniform and stable temperature (typically in the range of 20 ± 0.1–0.5 °C) and if error compensation is applied not only for deviations from the standardized 20 °C, but also for thermal gradients and transients that may occur around this temperature [58]: see standard ISO 1. It is essential to have a thermally stabilized CT machine and to allow time for the CT device and for any workpiece (!) to reach a uniform temperature of 20 °C (unless corrected). Few studies have been devoted so far to thermal stability and errors in CT measuring devices.

5.5. Scanning methods/measurement strategy

The general workflow and several aspects of the scanning strategy are discussed elsewhere in the paper: full scanning (360°) or partial scanning (180° or less, region of interest scanning, etc.), magnification, edge detection, GD&T analysis. This section elaborates on some specific aspects of strategy.

For CT nowadays two main scanning strategies are applied: rotation-only scanning with a cone beam, where the part is always inside the X-ray cone during the single measurement rotation, and slice-wise scanning with fan-beam based CT systems, where the part is measured in slices of finite thickness during each part rotation.

Further scanning modes are:

- *Rotation-translation scanning mode*. Here the part is translated through the X-ray beam under fixed angles of the rotary table. This technique was used more often in the beginning of industrial CT. It enables the measurement of larger parts, which do not fit in the X-ray beam with one pose. It requires substantially longer measurement times and is seldom used today. But it is worth noticing that this mode of operation is insensitive to certain types of artifacts which can affect rotation-only CT measurement: e.g. ring artifacts (Section 6.2).
- *Rotation-only scanning with offset*. In this scanning procedure the part's center of rotation is offset from the center of the X-ray beam. Thus, a fraction of the part is not within the X-ray beam but enters the beam during rotation. This mode of operation allows larger parts to be measured compared to the classical rotation-only mode, but suffers from a slightly decreased resolution and accuracy.
- *Rotation-only scanning with centered fan or cone beam* usually is operated with a set of projections covering a full rotation of 360°, while for parallel beam CT (at Synchrotron sources) 180° is enough. Cone or fan beam measurements are also possible with projections under *angles smaller than 360°*. A minimum of 180° is required. A smaller angular range decreases the measuring time, but worsens accuracy.
- *Helical scanning* originally has been developed for medical fan beam CT systems. Here the relative movement of the X-ray tube(s) and detector(s) to the patient describes a helix. This procedure has been adapted to industrial CT scanning also for cone beam CT. Helical scanning allows to lower measurement errors for faces of the workpiece which are parallel to the axis of rotation. It reduces Feldkamp artifacts (Sections 3.2.1 and 6.2) at the upper and lower boundary of the image (as with all fan beams). Its drawback is the higher measurement time compared to classical rotation-only cone beam scanning.
- *Rotation* of the part can be performed *step-wise or continuous*. With long measuring times these procedures virtually achieve similar results, but for high speed scanning (e.g. 1 rotation/min) continuous rotation causes movement blurriness.
- *Digital laminography* is a tomosynthesis method where projections of different poses are superimposed. Characteristic to this

method is either a relative rotational or translational movement of detector and source with respect to the object. Digital laminography uses dedicated reconstruction algorithms and is mainly advantageous for planar samples or parts with high dimensional aspect ratios. A drawback is limited resolution perpendicular to the assessed imaging plane [33].

Very recent scanning techniques try to overcome Feldkamp errors (Section 6.2) of classical cone beam based CT scanning. Here, rotation information of the part is added with translations.

5.6. User influence

The user of a CT system has a great influence on the result of the measurements as all industrial CT systems and GD&T software allow a wide choice of measurement parameters and strategy. The user influence starts with the system's warm up and potential waiting times for a settlement of e.g. thermal equilibrium of workpiece and CT system. The subsequent qualification of the system (calibration of pixel and voxel size, etc.) also includes user action and input. The setup and clamping of the workpiece also has influence as discussed in Sections 5.3 and 7.10.

Usually the parameterization of the measurement is also done by the user, possibly supported by software expert systems or predefined parameter sets. CT control software may have several user levels. Thus, users of limited skill can operate CT systems with only a restricted choice in parameters.

The user influence extends to choices of the postprocessing (e.g. filtering, thresholding, see Section 7.4) and the final geometrical analysis (Section 4.2). Obvious points of user input are (besides choices of procedures and parameters setting) choices of analysis or alignment regions and windows which can impact the reproducibility of measurement results and which also can contribute to systematic deviations of measurements.

6. Imperfections: artifacts and noise

This section describes unwanted effects that often disturb CT measurement. It also describes how to remedy or reduce some of those effects by proper selection of CT parameters.

6.1. Beam hardening

Beam hardening refers to the fact that – as the beam moves through absorbing material – low energy photons (i.e. soft X-rays) are more rapidly attenuated than high energy photons. So after a certain traveling distance into absorbing material, the soft X-rays will extinguish and only the hard X-rays will fully penetrate the part and reach the detector: the low energy X-rays vanish and the X-ray energy spectrum evolves to withhold only high energy rays (Fig. 19). So it looks like the first millimeter(s) of penetrated material absorbs more rays (soft and hard rays) than the interior part that only attenuates the remaining hard rays. This effect is clearly visible in the reconstructed CT voxel image (Fig. 20), where the outer skin of the workpiece appears lighter than the core and background (or darker if higher gray levels yield more absorbed photons, rather than more transmitted photons). This obviously will affect the part edge detection in general and the proper detection of material in case of multi-material components (see Section 7.5 and Fig. 25). Beam hardening (in combination with beam hardening compensation and scattering, see further) often results in barreling or cupping, which causes flat surfaces, of e.g. end gauges, to depict a barreled shape, while sharp workpiece edges are rounded off (Fig. 21).

A classical approach to remedy those flaws is to put a thin plate of e.g. Cu or Al in between the X-ray source and the workpiece to filter out the soft X-rays and to perform the CT absorption measurement with only the hard spectrum of the beam: see Figs. 6 and 19 for spectrum and Fig. 20 for result. Such physical filter allows a more stable and correct surface edge detection (using mid

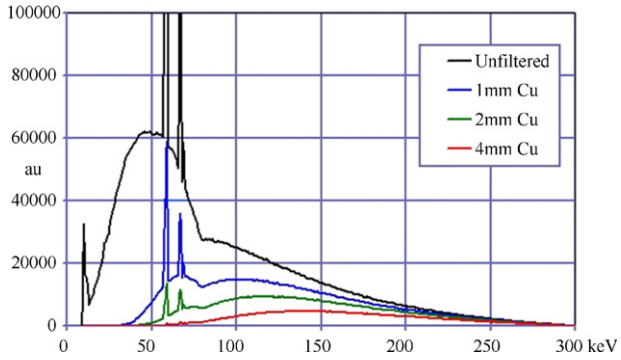

Fig. 19. Spectra at 300 kV. Effect of physical material filters to reduce beam hardening (filtering out low energy photons).

gray value or other thresholding method), but reduces the beam intensity and thus can worsen the S/N ratio of the assessed projections. This effect has to be compensated by an increase of the exposure and measurement time.

There exist further ways to correct for beam hardening:

- Assessment of non-linearity caused by beam hardening by the measurement of a step-wedge or a step-cylinder made from the same material as the workpiece. An alternative is to measure a plate made from the same material under several angles perpendicular to the axis of rotation. In any case, the correction is applied as a look-up table (LUT) to the assessed projections. This procedure does not work for workpieces of unknown material, but yields reasonable results also for not perfect material match (e.g. different aluminum alloys with moderate changes of non strong absorbing alloy content, i.e. Si, Mg, etc.). The drawback is the need of manufacturing, calibration and using the test specimen and the discrete nature of the correction (for step-wedges and step-cylinders) [28].
- Assessment of non-linearity caused by beam hardening by the analysis of the beam paths traveled through the workpiece and a subsequent correction of the projection. This procedure requires at least two reconstructions to be performed [50] or requires prior knowledge about the precise geometry of the part to be measured (CAD sketch of the workpiece) [31,50].

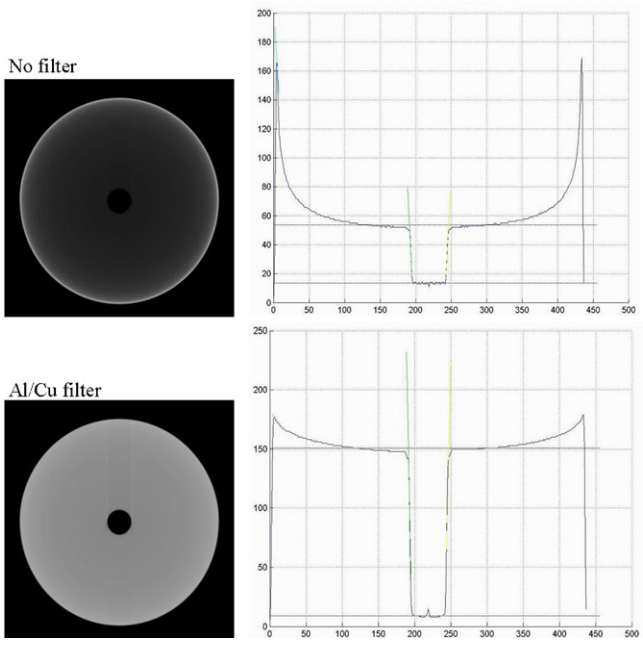

Fig. 20. Effect of beam hardening without and with a physical filtering of the X-ray beam. Hollow cylinder: outer ø 6, inner ø 0.6 mm [53].

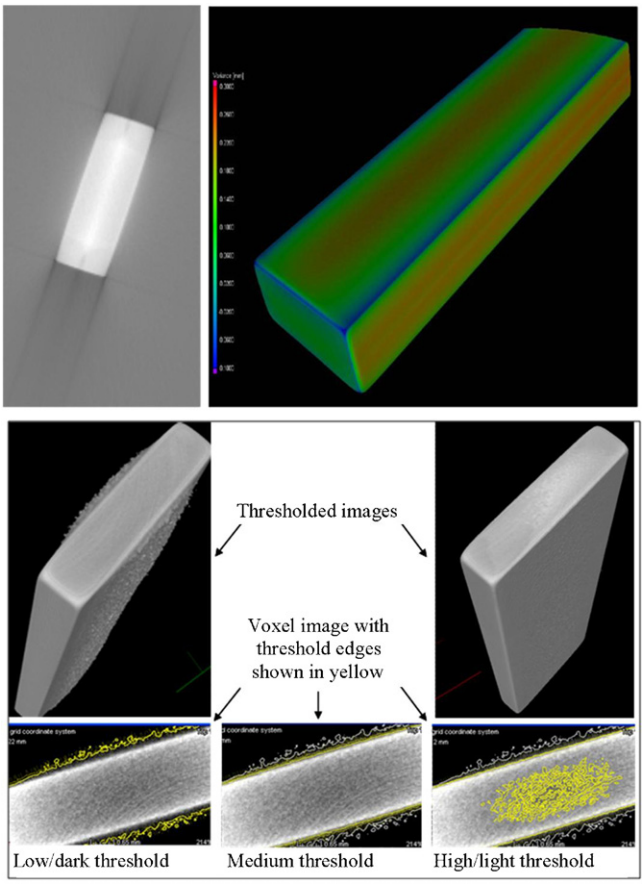

Fig. 21. Effect of scatter and beam hardening on a $Zr0_2$ end gauge (notice black artifact stripes on upper-left picture).

Many reconstruction softwares also offer different algorithms (e.g. polynomial correction) to numerically correct for beam hardening. Yet, filtering and correcting for beam hardening become quite difficult for measurements of multi-material components: see Section 7.5.

6.2. Other sources of imperfections: scatter, noise, geometric errors, etc.

Other disturbances are caused by physical phenomena or by the reconstruction algorithm:

- *Scatter* is caused by deflection of X-rays inside the workpiece material (see Fig. 16b), the detector or apertures. Some typical effects of scatter are shown in Fig. 21. Scatter often causes a halo without a dedicated structure at the location of the workpiece (Fig. 24) and reduces the S/N ratio locally. Values of scatter and of attenuation due to scatter can be found in literature: see Section 5.3 [68]. Several algorithms exist to reduce the effect of scatter and/or beam hardening (i.e. effect on attenuation). Those effects can also be reduced by proper thresholding (Figs. 21 and 24).
- *Ring artifacts* are caused by improper correction of non-ideal or defective pixels. These defects appear as rings of sharp contrast concentric to the center of rotation.
- *Metal artifacts* are caused by the presence of subvolumes with a much higher absorption compared to the rest of the part (e.g. steel insert in aluminum cylinder head). They appear as star like high brilliancy distortions inducing larger errors and inaccurate measurement near the metal components. Fig. 22 shows other high brilliancy ghost images appearing in the reconstructed 3D image due to the presence of high absorbing metal inserts in a glass/ceramic lamp.
- *Noise* is caused by quantization of X-ray photons itself, but can also originate from many other noise sources, e.g. electronic noise of detector or of amplification of signals.

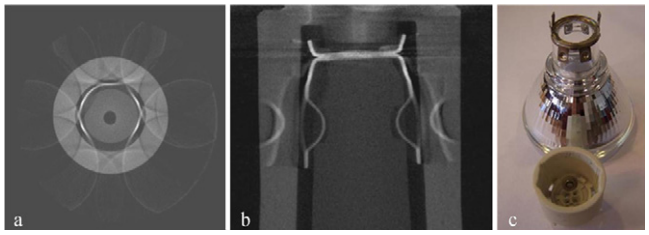

Fig. 22. Artifacts caused by metal inserts in lamp; (a) XZ section perpendicular to rotation axis; (b) section along rotation axis; (c) object.

- *Aliasing artifacts* are caused by the presence of part geometries that are larger than the field of view. Some literature also denotes artifacts due to undersampling at the level of image capture or reconstruction as "aliasing artifacts" [48].
- *Sampling artifacts* originate from discrete sampling of projections under restricted angular poses: see stripes on Fig. 10 at 4, 8 and 16 angles.
- *Filtering* (intrinsic): although physical filtering (see Section 6.1) may remedy some imperfections in the images, it will by itself introduce errors (e.g. scattering).
- *Rotation axis errors*: the rotation axis is supposed to be aligned parallel, resp. perpendicular, to the detector and its pixel rows or columns. Alignment errors are especially visible with high magnification measurements
- *Adjustment errors*: e.g. an oblique detector array not properly corrected during machine set-up may yield additional errors and artifacts
- *Error from wrong identification of rotation center*: at the beginning of the 3D reconstruction the software of the CT device will normally try to identify the location of the axis around which the part was rotated during CT image capturing. Failure in precise identification of the rotation center/axis will introduce reconstruction errors
- *Feldkamp errors* are due to larger cone beam angles and due to incompleteness of projections leading to distortions of the visible geometry (see Section 3.2.1).

For some of these errors, compensation or correction techniques exist (e.g. rotation center identification) which may either act on the projection images, or during or after reconstruction. Additionally, there are some techniques to reduce their impact by modifying the workflow of the measurement (e.g. a shaking movement of the detector during the rotation of the part to reduce ring errors).

7. Metrology aspects of CT

7.1. Measurand

All dimensional measurements using CT are based on the determination of the material boundary by the sequence of measurement steps described in Sections 3 and 4. Thus, the assessed surface geometry of the workpiece locally forms the measurand of the CT measurement. For a dimensional measurement this surface is further used for local or global measurement operations (e.g. point-wise measurement, fit of a regular geometry to a surface area or a global actual-nominal comparison against a reference data set). The quantitative description of the measurand for CT can be done by comparison to measurement results of other sensors or by simulation or analytical evaluation.

Aspects of interest which describe the measurand are:

- The uncertainty which has to be locally attributed to the measured surface, the spatial modulation of the measured surface in relation to the real surface of the workpiece.
- The uncertainty of measurement will be discussed in detail in Section 7.9. Concerning the measurand the uncertainty of measurement of CT is closely related to the question which

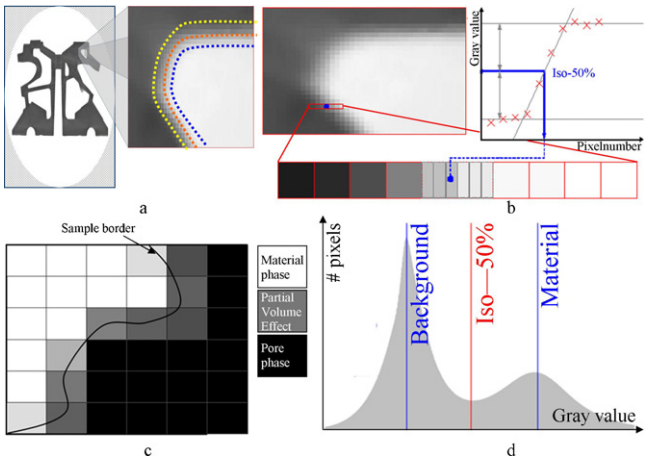

Fig. 23. Edge detection and thresholding [53,67].

sensor describes the surface best, i.e. which sensor or measurement methods can be considered as 'reference'.

The sampling of a surface by a CT measurement can be interpreted as a morphological operator which works on the surface geometry of the real workpiece. CT has intrinsically an integrative characteristic as it attributes an (average) gray value to a volumetric region (voxel) of the workpiece: see partial volume effect (Fig. 23). Tactile measurement with a probing sphere on the contrary has no integrating effect, but is linked to surface maxima (the probe measures on the tops of the surface roughness profile and an envelope is created by the finite probe radius), while optical systems use a kind of center line average roughness profile (unless partial transparency yields an offset inside the material). Hence measurement of a dimension (measurand) of a part with rough surfaces may yield systematic different results with CT, tactile and optical measurements [23].

A common approach to describe the morphological operator of CT is to state the modulation of a measured structure relative to the modulation of the real structure. This is expressed by a modulation transfer function (MTF) [ISO 15708-1 and -2]. The question of the modulation is closely correlated to the question which structure can be resolved and which structure can be measured with defined error limits. Further details on MTF and resolution will be discussed in Section 7.8.

7.2. Accuracy aspects

The measurement accuracy is influenced by:

- The *accuracy of the 2D X-ray images*, being influenced by the detector pixel size (Section 3.1.2), magnification, sharpness and contrast of the 2D images (Section 3.2.1), beam hardening and scatter (Section 6), etc.
- The *accuracy of the reconstruction of 2D images into a 3D model*, being influenced by the accuracy of the reconstruction algorithm (Section 3.2.1), the voxel size (to be selected by the operator), the accuracy in identifying the rotational axis (Section 6.2), beam hardening and scatter (Sections 6.1 and 6.2), accuracy of surface detection (Section 7.4), etc.
- The *errors* introduced when *dimensional measurements* are performed on the 3D model (influenced by the location and number of points used to identify the measurand and local coordinate systems, etc.).

This section focuses on accuracy of the first two steps referred to as 2D and 3D accuracy. It is however not always possible (nor essential) to isolate the accuracy associated to each of the three levels separately. Procedures exist to apply calibrated reference objects (e.g. calibrated grids) to calibrate the 2D image pixel size (which results from the physical pixel size of the detector and the magnification). Similarly, the size of the 3D voxels in the 3D model (which depends on the image pixel size, the reconstruction algorithm, merging of pixels, etc.) can be calibrated using 3D reference objects. In most cases however, length calibration is done globally: i.e. procedures are applied that directly identify global 3D scale factors by comparing lengths measured on a 3D reconstructed object model with known lengths of the measured object, thus covering the errors introduced at the three levels listed above. Distinction should however be made between the in-plane scale factor (rescaling in *XZ* rotation plane, Fig. 3) and out-of-plane scale factor (rescaling in *Y*), since both scale factors are influenced by other sources of uncertainties (reconstruction algorithm and artifacts, accuracy of *XZ*-rotation table or *Y* translation stage, etc.).

Some sources of errors were already described in Section 6.

The *2D image accuracy* is influenced among others by:

- Target material (Section 5.1)
- X-ray spot size (Fig. 8)
- Photon energy (source voltage) (Section 5.2)
- X-ray flux (source current) (Section 5.2)
- Exposure time (Section 6.2)
- Number of averaged pictures per pose
- Rotation speed and dwell/stop time (Section 3.1.3)
- Beam filter (material and thickness) (Section 6.1)
- Temperature (Section 5.4)
- Geometrical calibration of the detector
- Detector pixel size (resolution) (Section 3.1.2)
- Detector pixel repeatability
- Detector gain, sensitivity, etc.
- Magnification (Section 3.1.3, Fig. 8)
- Beam hardening and noise reduction algorithm (Section 6)
- Workpiece material (attenuation and scatter) or material combination (Section 5.3)

The *3D model accuracy* is influenced among others by:

- Accuracy and repeatability of CT kinematics (Section 3.1.3)
- Identification of rotational axis (Section 6.2)
- The selected voxels size (Section 3.2.1)
- Selection of *Y* increment (Fig. 3): number of slices
- Voxel and length calibration methods (Section 7.3)
- Reconstruction algorithm (Section 3.2.1)
- Beam hardening and noise reduction algorithm (Section 6)
- Edge detection algorithm and settings (Section 7.4)
- Workpiece material (attenuation and scatter) or material combination (Section 5.3)

The accuracy of the dimensional measurement assessment is influenced by the identification and definition of the measurand (Section 7.1) and by the common error sources affecting conventional coordinate measuring processes: influence of used measured points (amount, location, distribution, uncertainty on individual coordinates), datum definition (local coordinate system, reference features), etc. [100].

7.3. Pixel, voxel and length scale calibration (qualification)

As explained in Section 7.2, for each measurement, the length scale has to be defined in the in-plane (*XZ*) and out-of-plane (*Y*) direction: see Fig. 3. Those scale factors then account for the CT image magnification (*Z*-axis), the 2D pixel size (*XY* pixel size), the 3D voxel size (*XYZ* model size), and all other scale influences.

A common way to identify the *XZ* and *Y* scale factors is to measure a "3-ball artifact" (see Fig. 29i) together with the object to be measured: i.e. three small non-collinear spheres mounted on a base plate. Spheres are used as the identification of their center and distances is not influenced by edge thresholding and beam hardening. The two external spheres are generally positioned at approximately the same height in *Y* and used for *XZ* rescaling, while the middle sphere is positioned higher as to ensure an accurate *Y*-scale identification. It is highly advisable to perform this

3-ball qualification simultaneously to the CT measurement of the object, to ensure that the magnification factor (which is included in the scale factors and has to be accounted for in length measurements of the object) will be correctly included in the scale factor.

The material of the spheres (steel, ceramic, sapphire, ruby, etc.) is normally of little importance as edge detection offset does not influence the calibration. Nevertheless, ruby spheres mounted on steel rods (as used for traditional CMM tactile probe tips) should be avoided, as the presence of steel inside the ruby sphere may disturb the measured shape of the ruby sphere.

Other calibration artifacts can be used: e.g. "star probe" with five or tetrahedron with four ruby spheres on carbon shafts. Some of those will be discussed in Section 7.7. End gauges are not suited as they are very sensitive to scatter, beam hardening and barreling.

Another common way to rescale the measured object is to measure some lengths of the object on a tactile CMM, and use those lengths to rescale the CT voxel model and measurements. When using this method, care has to be taken to identify a proper edge threshold value first (or at least at the same time as identifying the scale factors, see [54] and Section 7.4) as inner and outer lengths are not independent from the threshold. Good scaling values can be assessed by measuring lengths which do not depend on edge thresholding and related effects (as beam hardening): e.g. measuring the length between two left edges of the parts.

Rather than using precise tactile or other measurements to identify the CT scale factors, one could also fuse tactile and CT measurements to morph the less accurate part geometry or shape, obtained with CT measurements, towards the more precise tactile measurement data: see Section 7.6 on data fusion and morphing.

7.4. Edge detection

Sections 3.2.1 and 4 introduced edge detection within the global workflow of CT measurements. Since edge detection is one of the critical and difficult issues in CT metrology and has a large influence on accuracy and traceability, this section further elaborates on it.

In medical and material testing CT applications, edge detection (also called segmentation) is often based on gray value thresholding: a certain gray value is assumed to coincide with the transition from one material to another. Due to the "partial volume effect" (edge voxels might contain more or less dense material, see Fig. 23c), inter-voxel interpolation is needed to locate the edge with sufficient accuracy within edge transition voxels [53,85]. This interpolation increases the resolution to sub-voxel resolution, but does not necessarily improve accuracy, unless a proper gray value calibration is performed.

The edge gray value is very dependent on the material being irradiated and obviously on the intensity of the radiation. A common method to identify a threshold gray value, that is less dependent on the radiation intensity, is to use the "iso-50%" value. This value is obtained from a histogram plotting the number of voxels versus the voxel intensity or gray value (see Fig. 23d). The histogram normally depicts a peak coinciding with each of the materials irradiated (including surrounding air or "background"). Iso-50% means that the mid-gray-value between the peaks is taken as threshold value. Depending on the number of voxels containing air and a given material, the peaks may largely differ in magnitude. Therefore, it might be appropriate to establish a histogram over a limited region of interest of the reconstruction volume in which material and background (or two different materials) are present to approximately the same amount. Verification tests with calibration objects have however demonstrated that the iso-50% threshold results in an edge that is often shifted with respect to the real material edge [54]. Tests done at K.U.Leuven show that a 50% threshold often results in aluminum parts being too small (optimal threshold lies around 35–45%, i.e. closer to the air gray value), while steel and $Zr0_2$ parts measure too large (optimal threshold for steel around 80–90%, i.e. closer to the material modus, and even further than the modus for $Zr0_2$). Fig. 24 shows the influence of the threshold value on measurements of steel and aluminum parts (look at shape, size and scatter noise).

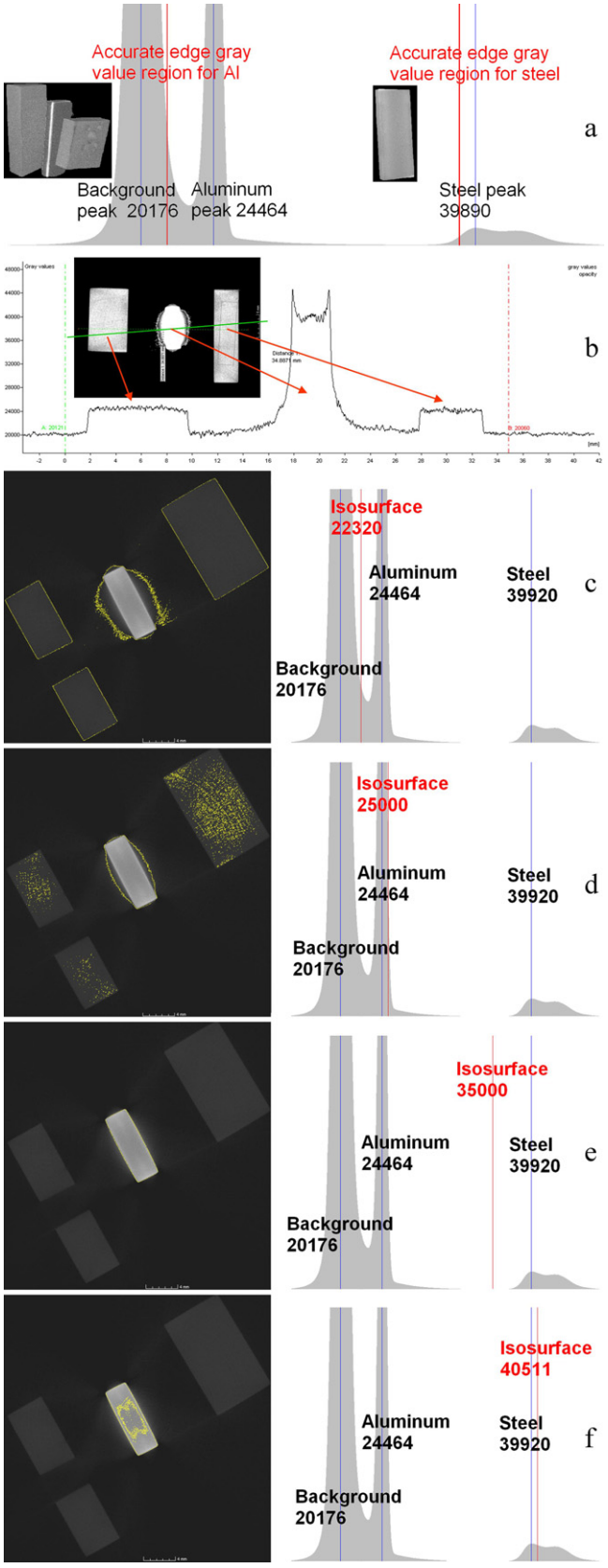

Fig. 24. Selecting threshold when measuring steel end gauge positioned between two aluminum parts: (a) optimal thresholds in red for steel (right) and alu (left); (b) gray value plot along green section line; (c–f) effect of shifting threshold–indicated with red Isosurface line and gray value level–from low to high value (look at yellow scattered dots).

Proper edge detection is complicated by beam hardening and other effects (preferably to be minimized before edge thresholding, see Section 6.1) and by the presence of multiple materials. In case of a component comprising two materials (M1 and M2) in air (A), the threshold value coinciding with the edge of material M1 will differ depending on whether it is surrounded by air or by the material M2: i.e. the thresholds for transition A–M1 and M2–M1 will have to differ. Applying iso-50% threshold between the peaks A, M1 and M2 does not yield good results: see Section 7.5.

Threshold values for a given material transition (e.g. A–M1) may be calculated and applied locally, rather than using global thresholding applying the same threshold over the entire workpiece: e.g. one could use a gray value histogram that only covers a local transition area including only the two materials considered for the transition threshold or calculate local maximum gray level derivative. However, this calls for long procedures, since accurate identification of threshold values generally requires comparing CT measurements (of the actual object or a calibration object made of the same material transitions) to calibration measurements of that object performed on e.g. a CMM machine. Several CT simulation software packages have been developed to identify proper CT settings (current, voltage, filter, threshold, etc.), but none provide an answer to this complex thresholding issue.

7.5. Multi-material measurements

Measuring multi-material objects (e.g. a plastic connector with metallic pins) yields typical problems related to artifacts and increased noise (Section 6), edge detection (Section 7.4) and measuring procedure (Section 7.10).

A first problem is to find an adequate threshold. Assume a combination of three materials having increasing gray levels L1 (air), L2 (rubber), L3 (steel): see Fig. 25 top-right [34]. At the transition between air (L1) and steel (L3), there will be some pixels having an intermediate gray level between L1 and L3 which will be wrongly recognized as rubber. Moreover, the optimal threshold (edge value) to distinguish steel from rubber may differ from the optimal threshold to distinguish steel from air. This is illustrated in Fig. 25 top-left and bottom, where steel and ZrO_2 end gauges have been alternated: putting the threshold at the iso-50% surface (i.e. middle) between background air and ceramic gray values will result in a different thickness for the ceramic end gauges when surrounded by air or by steel.

A second problem relates to proper selection of the X-ray power or energy when measuring different materials: high energy exposure (high voltage, current or exposure time) is needed to penetrate high absorbing material with sufficient photons reaching the detector, but does not allow visualizing low absorbing material (too little absorption). On the other hand, low energy exposure allows visualizing low absorbing material (if not fully absorbed by the high absorbing material), but will yield artifacts or total extinction due to presence of high absorbing material. Different techniques are proposed to solve this issue, among which multi-energy measurements fused at the level of 3D voxel reconstruction or of 2D projection images [56]. Multi-energy refers to measurements with different acquisition parameters, e.g. voltage (i.e. spectrum or photon energy), current or integration time (amount of photons).

This aspect has been widely investigated in medical diagnostic applications, e.g. for prostheses or amalgam fillings, but industrial applications are lacking behind. [55] uses two different X-ray spectra emitted by a high-energy (HE) macro CT source and a low-energy (LE) microfocus source. In order to combine the advantages of both measurements, the main object structure from the HE dataset is fused with the sharp edges of the LE dataset [39] using an adapted version of weighted arithmetic image fusion at the pixel level.

Another approach is based on fusing data sets from a single CT device differing only in the acquisition energy [76]. The method is based on manipulating the volumetric data and combining the two models via mathematical operations like averaging, etc.

Additionally it is possible to fuse on 2D projection level, i.e. two image stacks are acquired with different energies (integration time, current or voltage) and each pair of projections is combined to a new one [56]. This leads to a low-energy and a corresponding high-energy stack in which corresponding pixels of a single projection represent the same area of the workpiece. The workflow is shown in Fig. 26. This approach reduces noise in the data set as averaging of several projections would do, but requires less acquisition time.

In medical CT imaging gray values are normalized to the gray value of water (Hounsfield units). This decreases the energy dependency of visible gray values. Also multi-material analysis which is often standard for medical CT imaging is relieved. Due to the fact that industrial CT-measurements usually are not normalized, the comparison of different CT measurements on voxel level often appears difficult. Thus, normalization is desirable and can be an improvement for certain analysis and measurements also for industrial CT.

7.6. Accuracy improvement by data fusion

Accuracy of CT measurements can be improved by data fusion. One can fuse different CT measurements taken at different magnitudes or positions/orientations in the work volume of the CT device [81] or taken at different energy levels [56]. The latter might be appropriate for measuring multi-material parts (see Section 7.5) or parts with high aspect ratios, requiring high energy for full penetration of the long side of the part and low energy to avoid scatter or overexposure along the thin side.

Another possibility is to use measurements performed with more accurate sensors (tactile, optical) to reduce systematic deviations of CT measurements [25,93,95]: Fig. 27. Tactile or optical measurements are generally more accurate and are usually

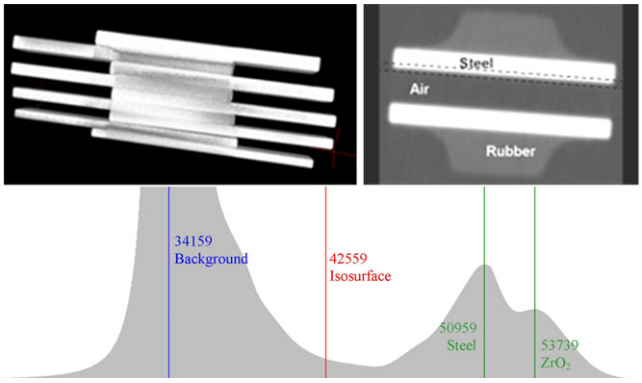

Fig. 25. Multi-material measurements: top-left and bottom apply to alternating steel and ZrO_2 end gauges; top-right is a steel sleeve surrounded by rubber.

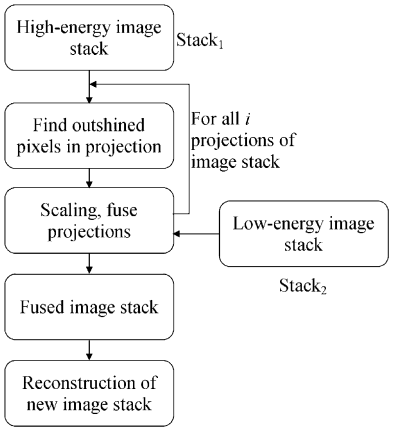

Fig. 26. Workflow of CT image stack fusion [56].

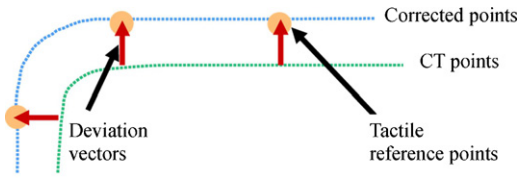

Fig. 27. Example of a corrected CT point cloud using tactile points.

approved with length standards traced back to the national length standard, e.g. using ISO 10360. A proper interpolation of correction vectors might require a dense assessment of the outer geometry of the workpiece with a tactile or optical sensor and a treatment of the interpolation errors between the measured points. Fusing data of CT and tactile or optical sensors allows improving the CT measuring accuracy (to values below 5–10 μm) and to perform more accurate holistic measurements of the entire workpiece: i.e. to use CT to acquire dense volumetric data representing not only the outer surface but also the interior and conventionally not accessible features (undercuts) and to correct outer and inner CT measuring data using more accurate tactile or optical measurements performed at the outer side of the workpiece. Fig. 28 shows the workflow of the correction procedure. The procedure might be cumbersome for single part measurement, but is well suited for measuring a series of parts. In this case, only the first part or a reference part has to be measured with a tactile sensor and the calculated deviation vectors are stored for future tomographies of similar workpieces. These corrections account for the sum of all influences yielding systematic geometric measuring deviations (beam hardening artifacts, scattering, scaling errors and others) and may be used when measuring similar parts. The procedure proved efficient for measuring plastic connectors of metallic injection nozzles with measurement uncertainties <1 μm [75].

Alternatively, fusing CT and tactile CMM measurement is suited for (re)calibrating CT images or models in the *XZ*-plane and in the *Y*-direction (see Section 7.3). The rescaling may even be more adaptive and dependent of orientation or shape. Typically, the outer geometry of a part, obtained from CT measurements, could be rescaled or morphed using tactile measurements taken on the outer faces of the part. The inner geometry (that is inaccessible to a tactile probe) may be corrected by congruent morphing with the outer geometry. But this extrapolation may suffer from physical effects which are not treated adequately by a simple extension to inner regions of the workpiece.

7.7. Accuracy specification, verification, correction and qualification

Today there is a lack of well defined reference objects (also called metrological artifacts) and procedures suited to assess the accuracy of CT-based CMMs, to compare the performance of various CT measuring devices or to calibrate errors of CT CMMs in view of subsequent error correction. This situation contrasts to that of tactile

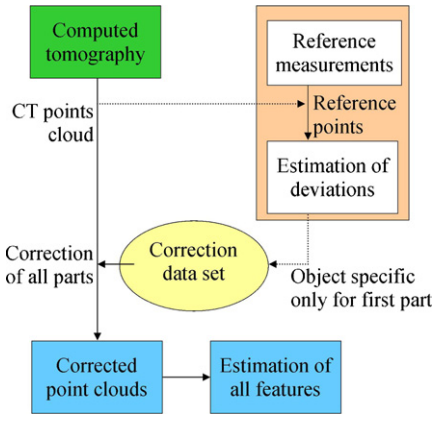

Fig. 28. Workflow of correction procedure [95].

and optical CMMs for which suited artifacts and procedures already exist and have been partially standardized, e.g. in the ISO-10360 standard suite. However, the latter standard is not directly applicable to CT-based CMMs. ISO 10360 is typically made for CMMs where we can distinguish between the length measuring system of the CMM (i.e. the linear or rotating measuring scales integrated in the displacement axes of the machine and used for calculating length displacements) and the measuring probe or sensor (i.e. tactile probe or single point laser triangulation probe used primarily for aiming at a specific point whose coordinates have to be identified). ISO 10360 therefore requires a separate qualification of the accuracy of the length measuring system (maximum permissible length error MPE_E) and of the probe (maximum permissible error of the probe MPE_P). The length measuring error E_L is based on 2-point length measurements performed on calibrated end gauges or step gauges (L_a) that are compared to the known calibrated lengths (L_r): $E_L = L_a - L_r$. MPE_E defines an envelope that should contain all E_L values. The standard requires measuring E_L-values for five independent lengths along the three Cartesian coordinate axes and along the four main diagonals of the CMM. The probe errors are based on a limited set of discrete points measured on a calibrated sphere: ISO 10360 advices to measure 25 points on the sphere and to calculate the deviation between measured and calibrated diameter ($P_S = D_a - D_r$), together with the variation on the measured radius in the 25 points ($P_F = R_{max} - R_{min}$). In CT CMMs, one cannot distinguish between the CT probe and the length measuring system of the CMM. Measurements cannot be done along Cartesian measuring axes or along diagonals to those non-existing axes. Moreover, in CT, measuring reference lengths of gauge blocks does not rely on two point measurements defining length L_a, but is usually calculated using two fitted elements (planes) resulting from a multitude of points thresholded on faces of the gauge blocks. In CT CMMs, point probing and length calculation are interwoven and cannot be separated, and the measurements are done in such a way that ISO 10360 cannot be applied as such. There is a need for new procedures and standards, not only for accuracy specification and verification, but also for identification of individual error components (compare to identifying 21 geometrical errors of Cartesian CMMs using laserinterferometers, lasertracers, step gauges, ball bars or plates, etc.). The German guideline VDI/VDE 2630-1.3 (or VDI/VDE 2617-13) is currently the only standard for CT CMMs. It proposes applying the error parameters of ISO 10360 ($MPE_{E/P}$, E_L, $P_{S/F}$) but adapted to CT, and it forms the basis for further discussions [90].

Different test or reference objects have been proposed for CT CMMs [9,32,54,89]: see Fig. 29, artifact a–m. These metrological standards often aim at different purposes: see below.

A first set of reference objects are inspired from metrological standards designed for conventional CMMs. They have the advantage of being similar to commonly accepted CMM standards (hence allowing intercomparison and use on different types of CMMs [27,36]). However, they may often not be well suited to verify (in)accuracies or to calibrate CT scanners. Examples of such standards are [89]:

- Standards with reference spheres, like ball bars or assemblies of ruby spheres (Fig. 29, artifacts b, h, i, k), allow point-to-point distance measurement and are well suited for calibration of CT scale factors, because the measurements of the positions of the spheres are not influenced by edge detection, thresholding, beam hardening or surface offset. On the other hand, they are less suited for calibration of the threshold value, because the material of the sphere (ruby, steel, alumina, zirconia) often differs from common workpiece materials (plastic, Al, Ti, steel) and the spheres are generally quite small (compare to step cylinder below). Standards combining several CMM probe tips (ruby spheres mounted on steel rods) often yield problems due to the high difference of absorption between the steel rod and the ruby sphere material. Better alternatives are spheres mounted on carbon fiber rods (artifact b, h, k) or glued to a carbon plate. Measuring a large set of inter-sphere distances of different length

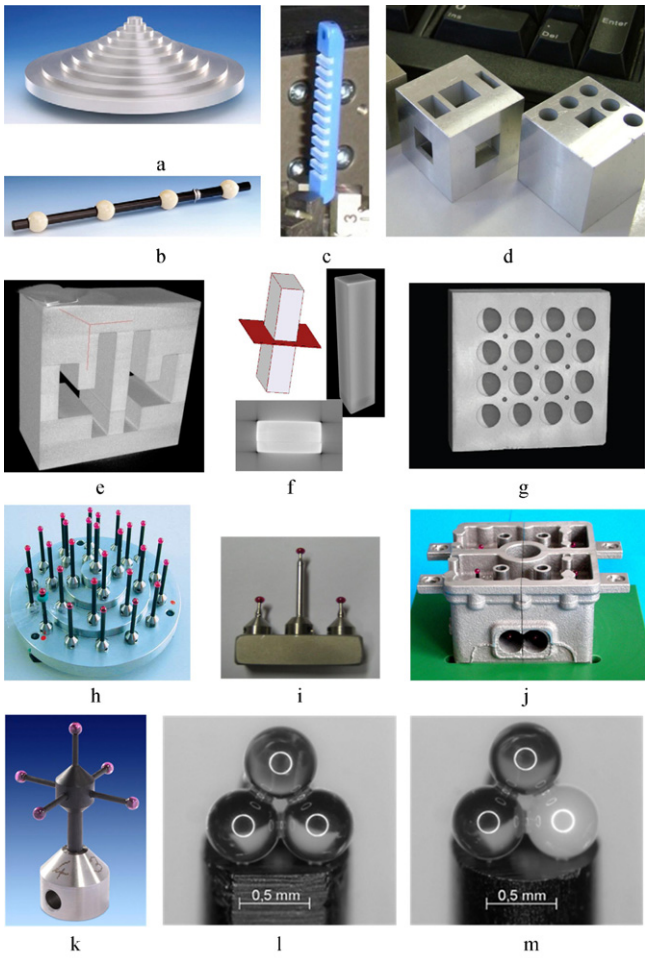

Fig. 29. Test standards for CT metrology.

(e.g. using artifact h or using a calotte artifact, see below) allows to verify or assess the Maximum Permissible Error of length measurements (MPE_E). In [32] a MPE_E is reported of $MPE_E(\mu m) = 2 + L(mm)/90$. Other manufacturers report a MPE_E of $5 + L/50$ [61,103] and $4.5 + L/75$ [98]. However, one should realize that such MPE_E-value often is an embellished accuracy estimate, as the reconstructed position of the spheres' centers does not suffer from threshold errors (offset errors), nor from measurement variability (due to the averaging effect of using many surface points to calculate one coordinate). Notice that this holds for all standards using cylindrical or spherical reference features: accuracy turns to be an order of magnitude better than for distance measurements based on single point probing (e.g. using end gauges or step gauges, see Fig. 29 artifacts c, d, e and f). VDI/VDE 2617-6.1 and 2617-6.2 for optical CMM measurements and VDI/VDE 2630-1.3 (also VDI/VDE 2617-13) for CT offer a procedure to correct pure measurements of sphere centers to assess a real bidirectional length measurement error. In this procedure, the assessed numbers also contain the influence of potential threshold and other local errors. It is recommended to check how any statement of MPE_E has been assessed.

- The 2D calotte plate [9] and 3D calotte cube [66] proposed by the Physikalisch-Technische Bundesanstalt PTB (Figs. 29g and 30c) are inspired from ball plates or cubes and hole plates often used for calibrating 2D or 3D tactile or optical CMMs [27]. They allow mapping 2D/3D deviations [3,74] and defining CT rescaling factors. However the way they have to be used for calibration and error compensation is quite different for CT devices. A 2D calotte array may be used for calibrating 2D flat panel detectors. 3D error mapping or calibration is something else: in CT devices those objects are rotated rather than being aligned to the Cartesian CMM coordinate system and are therefore not suited for 2D/3D error mapping of the measuring volume. Nevertheless, 2D or 3D plates can be used for the testing of CT systems and can identify residual anisotropies within the measurement volume.

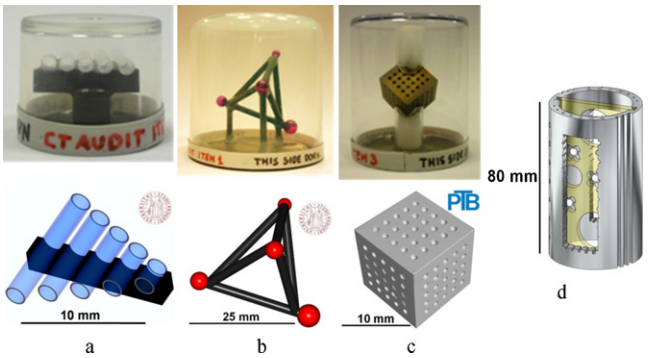

Fig. 30. Four standards used within the international "CT Audit" intercomparison [20].

Some other proposed standards are:

- A step-cylinder (artifact a, possibly with a central or stepped bore inside) is suited to calibrate (rescale) external (and internal) measurements. It is well suited to adjust the measuring parameters versus material-specific absorption and penetration thickness. Analyzing the circle diameter and shape deviation [65], it also allows detecting the maximum possible material thickness. However, it does not involve point-to-point distance measurements. Hence it is less suited for accuracy verification and for scale factor mapping (calibration) and correction. Standard types of step-cylinders without inner bore do not involve internal measurements and hence does not allow to separate edge detection offset errors (threshold errors) from scaling errors. Step-cylinders with a central bore, as proposed in VDI/VDE 2630-1.3, allow this kind of analysis. The VDI/VDE guidelines define several accuracy characteristics for such artifact (G_S, G_F, G_G) for size, form and straightness. Step and simple cylinders can, according to e.g. ISO 15708, also be used to check the modulation transfer function (MTF) of the CT system under study.
- Standards with plane-parallel surfaces (end gauges (f), step gauges (c) or prismatic standards (c, d, e, f)) are more representative of the accuracy obtained in point-to-point or face-to-face length measurements, as they do not involve center point averaging as with circles, cylinders or spheres. They may be critical in assessing the barreling effect that deforms flat or non-uniform curved surfaces due to beam hardening and cupping effects. That may yield to major measuring inaccuracies. Ideally, the standard should contain external and internal features (see artifact c, d and e) to assess the possibility to measure internal features and to distinguish between scale errors (calibration of pixel/voxel size and magnification) and offset errors (edge detection and threshold) [54]. Using different wall and air gap widths allow a better assessment of the thickness effect, as the errors may change with wall and air gap thickness. Artifact e – the so-called "cactus step-gauge" – has steps of 5 mm (at least in the middle zone of the standard). It can be produced relatively easily in various materials (e.g. in the specific materials of the parts to be measured). Thus it allows accounting for material specific issues during accuracy verification (e.g. material dependent thresholding). Tests with crenellated multi-material step gauges, alternating steel and ceramic end gauges of identical or different thicknesses, have been performed at the University of Leuven, but still face measuring problems.
- Some accuracy verification objects aim to represent real work-piece geometries. GE/phoenix used an airplane aluminum valve manifold from Continental to check the accuracy of CT devices [32]. PTB uses a segment of a cast aluminum cylinder containing reference elements (4 inserted spheres, 2 outer cylinders, 5 inner

cylinders and 3 planes): Fig. 32a [6,9]. PTB and BAM developed another workpiece-like reference object: a smaller cast aluminum cylinder head dismountable into 4 segments and modified with reference elements (3 spheres and cylinders) for each segment (Fig. 29j) [11,81]. For analyzing multi-material properties of CT, one segment has been substituted by another material (here plastic) [12]. All those workpiece-like objects feature freeform geometries or complex features to be measured by CT. Proper calibration is required to assess the geometry of the objects in a correct and traceable way [11] (see Section 7.8).

- PTB has developed a scalable reference object: tetrahedron with 4 spheres mounted by micro-assembly [62]. When made from the same material (4 ruby spheres, Fig. (29, artifact l) it can be used to assess scaling factors [79] and to test CT systems. Specimens with spheres of different materials (3 ruby and 1 ZrO_2 spheres, artifact m) are suited to check and further develop edge-detection for multi-material applications [6,79]. Currently micro-tetrahedrons are the smallest available reference standards and have been manufactured down to a sphere diameter of 0.127 mm and tested with synchrotron CT [80]. Calibration of micro-tetrahedron with spheres down to 0.5 mm can be ensured using tactile micro-CMMs [79].
- Fig. 30 shows the four calibrated standards used for the "CT Audit" inter-laboratory comparison on CT for dimensional metrology, organized by the University of Padova and using standards of this university, PTB and QFM [20].
- Other standards have been proposed. Carmignato et al. propose a standard for testing micro-CT systems, based on glass fibers mounted onto a multi-holes polymeric ferrule. Holes and fibers have nominal diameters equal to 125 μm [22].

Any conformity testing performed with calibrated standards (e.g. using standards of Fig. 29 or 30) has to be evaluated according to the rules of ISO 14253-1 [42]: i.e. the uncertainty of the measurement has to be considered for making a conformity statement (e.g. towards MPE-limits). In case of tests performed by an independent tester, e.g. a service provider, this uncertainty is the test uncertainty according to ISO 23165-1. Most important uncertainty contributions – among others – are the calibration uncertainties of the calibrated standard and those due to incomplete knowledge of the coefficient of thermal expansion of the calibrated standard (if a compensation of thermal effects is performed). For CT-measurements, at least these two influence factors have to be accounted in the stated uncertainty. Further contributions are described in ISO 23165-1, but may have to be reconsidered for the case of CT, e.g. difference between calibration strategy for a calibrated standard and the measurement strategy for its use as testing standard. Care should also be taken as vendors of CT devices may propose artifacts in "cooperative" materials and geometries that minimize the impact of the material or geometry during the qualification test.

7.8. Resolution

One should clearly distinguish between accuracy (as characterized in Section 7.7) and resolution of a measuring device. High resolution is not synonymous of high accuracy and vice versa.

Resolution can be defined as the smallest detail (step or feature) that is still perceptible or inducible within a machine: e.g. the smallest displacement or change of length that can be identified on an analog or digital readout scale, or the smallest inclusion that is still perceptible on an optical or X-ray image sensor. For CT devices, one should distinguish between the resolution or smallest perceptible detail within 2D X-ray images and the resolution or smallest perceptible detail within a 3D reconstructed CT voxel model. The X-ray 2D image resolution is often characterized by using thin wires or thin wedged slits as artifact to check for the limit of perceptibility.

For optical and X-ray devices the term structural resolution has been defined to describe the ability of the system to transfer a feature modulation present at the input of the system to the output within definite measurement error limits. Although low-pass filtering decreases the probing deviation for form by suppressing noise of the measurement points, it worsens the structural resolution for dimensional measurement [22]. Hence this resolution has to be determined and indicated in addition to the characteristics described in Section 7.7.

Distinction should be made between several definitions of resolution. *Spatial resolution* is well defined for optical sensors as the axial resolution defining the smallest measurable displacement along the direction of measurement. *Structural resolution* is defined here as the smallest structure measurable with maximum permissible error to be specified. In contrast to spatial resolution it is not included in the error indicating size measurement and probing error (MPE_E or MPE_P). As structural resolution is influenced by low-pass filtering, the probing error improves while structural resolution deteriorates [90].

The *spatial resolution* or *structural resolution in voxel gray value domain* can be determined according to EN 62220-1 in radiography via the modulation transfer function (MTF): see ISO 15708. Not only the interpretation of these values is difficult, but the use in CT is limited as this definition does not cover the entire process of CT measurements: the method to determine the structural resolution should obviously include the entire workflow used for dimensional CT measurements, i.e. especially reconstruction, surface extraction and filtering operations.

The draft guideline VDI/VDE 2630-1.3 describes a comprehensive method to determine the *structural resolution for dimensional CT measurements* D_g which is defined as the diameter of the smallest usefully measurable sphere. This definition directly indicates the performance of the device to measure small workpieces accurately rather than only indicating a simple perceptibility. As spherical calibration standards are used, the definition of different resolutions for different directions is not necessary. Therefore a calibrated sphere, e.g. a tactile stylus, is used. The measurements of the calibrated sphere have to take into account all parameters and settings typically used for the evaluation of the MPE_P and MPE_E values. The structural resolution has to be defined and measured for each magnification; the according values for P_S and P_F have to be indicated.

It is vital to cover the entire sequence of CT measurements while determining the structural resolution: i.e. structural resolution for dimensional measurement should be distinguished from structural resolution in voxel gray value domain which does not contain surface extraction. A good structural resolution in voxel domain will have a positive effect on dimensional measurements but it is not sufficient for good measurement results. The definition of resolution solely on base of the voxel size is not justified: the structural resolution for dimensional measurements will typically be much worse, while the measurement uncertainty (see Section 7.9) of e.g. larger structures (e.g. center of spheres) can have a value smaller than the voxel size.

Notice that discussion on structural resolution and its harmonization for CT, optical and other sensors is not finished yet.

7.9. Measurement uncertainty

The only characteristic describing the quality of a specific measurement result is the measurement uncertainty. Each measurement result should be provided with its uncertainty in order to ensure that the measurement is traceable to basic SI units (here the unit of length–the meter) and to state the conformity or nonconformity to tolerances [42]. A dimensional measurement (CT or other) has to include a correct statement of the task specific uncertainty [100]. The general reference method is outlined in the Guide to the Expression of Uncertainty in Measurement (GUM) [43]. However, as seen in Sections 5, 6 and 7.2, uncertainty in CT measurements comes from many sources. Calculating the total uncertainty of CT measurements is hence quite difficult due to the fact that CT systems are multi-purpose measuring devices whose

uncertainties vary with the task being performed, the X-ray source settings, the workpiece geometry [59], material, position and orientation, the detector, the environment, the operator, the data evaluation algorithms and parameters, the chosen measurement strategy, etc.

Important for CT measurement uncertainty is the value to which any statement refers: i.e. which is the measurand to be measured (Section 7.1) and what is the reference method for making any uncertainty statement. Usually, tactile probing of a surface is set as reference. When using this definition for CT, one has to keep in mind that tactile probing of e.g. a rough surface performs a morphological filtering of the surface profile by the probe tip (influence of probe radius) and an offset of this profile (offset towards roughness peaks), and thus does not reveal the "real surface".

Up to now there are no international standards or guidelines concerning the evaluation of uncertainty in the specific case of CT measurements. For this reason, and also due to numerous influencing factors and their complex interaction, industrial users of CT systems are typically not able to provide appropriate statements of CT measurement uncertainties [21]. Since the measurement uncertainty strongly depends on the measurement task and the measurand definition, the use of specifications for assessing the task specific uncertainty (e.g. according to the draft VDI/VDE 2617-11 standard) is not adequate for CT measurements [5]. Several research institutes and technical committees are presently working in the field of CT measurement uncertainty evaluation. In 2004, for example, the Technical Committee VDI/VDE-GMA 3.33 has started working on the guideline VDI/VDE 2630 "Computed tomography in dimensional measurement" [89–91]. The Committee is now working on uncertainty evaluation methods for CT measurement data (VDI/VDE 2630-2.1 Draft 2011).

Different approaches for uncertainty determination of industrial CT measurements are applicable [4,17,43,44]:

- expressions for analytical calculated uncertainty budget (standard GUM method using error propagation theory) [43],
- variability simulation (e.g. Monte-Carlo statistics) [44],
- experimental determination of systematic and stochastic variability (ISO 15530-3 [45]),
- expert knowledge and assessment,
- combination of previous methods.

The standard method is to calculate the measurement uncertainty through an uncertainty budget according to GUM [43]. This requires an evaluation model that collects all input quantities influencing the value of the measurand and that specifies the effects of changes of each input quantity on the measurand (error propagation theory). Due to numerous influencing factors (see Sections 5, 6 and 7.2) and the lack of any self-contained theories for modeling their influence, the most complicated part in the GUM procedure is to set up the analytic equations considering all relevant input quantities. Consequently, even though the GUM is the principal document for consistent evaluation of measurement uncertainty, this method alone has not been applied to determine the total uncertainty of CT measurements: formulating a classical uncertainty budget actually requires extensive work or is even impossible for most CT measurement tasks [97]. Only simplified studies have been conducted so far [94,96].

Variability simulation (Suppl. 1 to GUM [44], ISO/TS 15530-4, VDI/VDE 2617-7) is an elegant alternative to uncertainty budgeting. The approach is well suited for very complex measurement tasks such as CT measurements. Like the standard GUM method, it requires profound knowledge of the measurement chain and the statistical distribution of each influence quantity. The uncertainty evaluation is then not performed analytically, but through numerous simulated samples in a virtual experimental set up, similar to the "virtual CMM" approach for tactile CMMs. Monte Carlo algorithms are often used for the simulation [59,100]. A number of approaches using Monte Carlo algorithms have been developed to simulate radiographic and CT imaging processes for

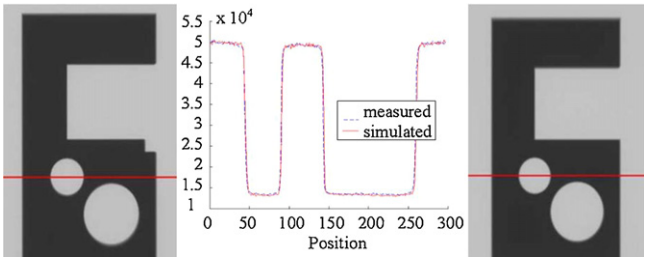

Fig. 31. Example of comparison between real (left) and simulated projection data (right). The comparison of gray value profiles (middle) shows excellent correlation between the two datasets [51].

industrial purposes [46,47,57,73,86]. The first examples applying a simulation approach for estimating measurement uncertainty for simple geometries are reported in [40,51,97]. In these publications, comparison of measured and simulated CT data is achieved by developing a specific deterministic software tool for simulation of the CT image acquisition process. The simulation results are found to agree well with authentic X-ray projection images. An example of comparison of measured and simulated CT data is shown in Fig. 31. Measurement uncertainty could be determined through a combination of deterministic CT simulations and Monte Carlo variation simulations of influencing quantities.

Another approach for determining uncertainties due to influence quantities and their interaction is the use of experimental methods such as those applicable for CMMs and described in ISO/DTS 15530-2 and ISO/TS 15530-3 [45]. ISO/DTS 15530-2 describes a procedure to estimate the task specific measurement uncertainty from multiple measurements of the workpiece positioned in different orientations and locations of the measurement volume. In CT measurements, results are strongly dependent on the workpiece orientation and in some cases also on its location. Therefore, measurements in completely arbitrary orientations are not a good representation of actual CT measurements by skilled operators. Hence, only changes within reasonable limits should be applied to orientation and location of the workpiece. The procedure that involves the utilization of calibrated workpieces according to ISO/TS 15530-3 is currently regarded by many authors as the most promising for CT measurements [8,19,23,26,78]. The procedure is based on a sequence of repeated measurements of a calibrated workpiece using the same strategy and the same conditions as actual measurements performed on the part to be inspected. The calibrated workpiece used in the procedure must be of similar material, size and geometry as the actual part to be measured. The differences between the results and the known calibration data are taken into account for the uncertainty calculation, together with the calibration uncertainty, the repeatability of the measurement process and the influence of the workpiece. The uncertainty influence of software, the applied workflow and the user impact should be covered by the repeated CT measurements, at least to the extent that they are not constant and do contribute to variability in the measurements. Otherwise an underestimation of the measurement uncertainty may occur. The influence of analysis intervals and selections can be analyzed with traceable measurement software which provides an easy way to execute an analysis with modified input parameters and with changed parameters of the processing chain. Several similar (uncalibrated) workpieces should be measured additionally if one wants to take into account the influence of variability of the workpiece geometry or material. The study of the measurement uncertainty should also cover the influence of registration of data sets.

A critical aspect to the application of ISO/TS 15530-3 to CT is the missing guidance in dealing with CT specific effects. Consequently, effects specific to CT that are present in particular measurement tasks must be taken into account additionally. For example, the strong influence of material and roughness of the workpiece must be considered [30]. Several research works have proven that the experimental approach using calibrated workpieces is a suitable

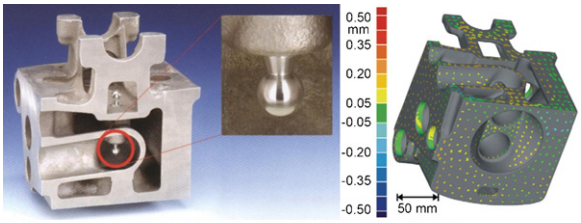

Fig. 32. Cast aluminum cylinder head segment with reference elements (a). Local CT measurement errors (b). The segment was calibrated at 3059 points using a tactile CMM [9].

approach for CT uncertainty evaluation. This was demonstrated on different calibrated objects, e.g.: step cylinders, ball bars, titanium calotte cubes, aluminum cylinder heads and other aluminum parts [8,9,41,78]. For example, Fig. 32b shows the results obtained from the comparison of CT measurements and CMM calibration of an aluminum cylinder head segment. VDI/VDE 2617-8 offers an approach for including some of the CT specific effects to an uncertainty study by measuring a set of uncalibrated workpieces additionally to a calibrated workpiece. A cumulated standard deviation of the measurements of the uncalibrated workpieces finally enters into the uncertainty calculation.

An important point with the use of ISO 15530-3 (and VDI/VDE 2617-8) is the influence of systematic errors. The GUM strongly recommends to correct systematic errors present in measurement results. It proposes to calculate variability propagation only for cases where such correction is not applied, i.e. for unknown systematic errors. But, ISO/TS 15530-3:2004 and VDI/VDE 2617-8 (2006–2007) do not use this GUM conformant approach. Thus, the used formula has to be correct and applied in a GUM conformant way [37]. For the case that systematic errors are corrected according to the recommendation of GUM, the uncertainty of the correction, which is not covered by the repeated CT measurements, has to be added to the uncertainty statement. An influence not covered by the repeated CT measurement is the influence of the incomplete knowledge of the coefficient of thermal expansion of the calibrated workpiece which has been used to assess the correction value. The issues described above will enter in the new revision of ISO 15530-3 which is under development.

In former times, as there were no means to measure internal part geometries, designers refrained to construct parts with functional internal shapes having critical tolerances. This is changed by the advent of CT. But knowledge of measurement uncertainty of these measurements is required to enable e.g. conformity statements according to e.g. ISO 14253-1.

A possible approach for assessing the uncertainty for CT measurements of internal geometries is the use of a dismountable workpiece-like reference standard, e.g. a cast workpiece cut into segments in which reference spheres are mounted (Fig. 29j) [11,81]. The part can be calibrated in the dismounted condition (e.g. with an accurate CMM) and can be measured with CT in the assembled state. Thus, the CT measurement deviation and therefore the CT measurement uncertainty can be assessed for external and for internal geometries. This procedure can yield valid measurement deviations under the condition that the geometry of the modified part (cut into segments and modified with reference geometries, e.g. spheres attached to each segment) is close to the geometry of the real workpiece. This condition is valid for all procedures relying on the approach of ISO 15530-3. Cutting the part has to be done with control and minimum removal of material. Thus, EDM cutting has been applied [11]. Additionally the change of geometry induced by the cutting should be controlled by CMM and CT measurements before and after cutting. Therefore, it is beneficial to apply at least 4 spheres to each segment as this results in a set of 6 reference lengths where a potential impact on one sphere can be detected. Additionally, 4 or 5 spheres per segment can be used for more stable registration of data sets. The uncertainty on the registration of data sets should be included in the uncertainty statement.

A drawback of the experimental approach using repeated measurements is that it can be time consuming due to long measurement times and the number of repeated experiments needed for statistical validation. This is relevant especially when the effect of several influence quantities has to be investigated. However, knowledge of the contribution of each factor is not required in the experimental approach, as only the overall variance of the measurement result and the systematic error of the calibrated feature are actually necessary. To reduce extensive experimental effort, experimental analysis and simulations can be combined as exemplified in [78].

Actual to nominal comparisons are required for analyzing the measurement uncertainty. But if single points, e.g. data points from a tactile CMM measurement are compared to a CT measurement (i.e. a surface model) the analysis must be made using the surface normal of the real part for correct comparison. This requires the normal to be assessed in a traceable and correct way. For the comparison, the CMM data (point and normal) must be set as reference while the CT data set is set as actual. This procedure requires both, a traceable and correct assessment scheme which also works for parts with stronger deviations to a CAD model, for parts with significant roughness and high local curvature [11]. Additionally, the inspection software must be able to work with 6D datasets (point and normal) for inspection purposes of surface data [11]. Probing techniques for a stable probing of complex freeform surfaces can be improved by a local fit of an appropriate model to sampled surface data points [7]. Only in the cases where it can be assured that the local curvature does not impact the comparison, the reverse (incorrect) procedure may be possible: i.e. to set the CT measurement as reference and the tactile data point as actual. Up to now this is the industrial standard (without any care whether this is justified or not).

Various studies demonstrate that sub-voxel measurement uncertainty can be achieved in dimensional CT measurements that take correction of specific systematic errors into account [5,9,16,41,54,78]. Data comparing the actual accuracy of different CT systems are rarely documented in literature. This is due to the lack of international standards for CT metrological performance verification and, hence, different CT systems manufacturers provide different specifications based on dissimilar terms and procedures [60]. In order to map the current quality of CT measurements and to compare measurement results from different CT measuring systems among each other and with reference CMM measurements, the "CT Audit" interlaboratory comparison, organized by University of Padova, is currently running (see Fig. 30 and www.gest.unipd.it/ct-audit) [21].

7.10. Good practice measuring procedures

The quality of dimensional CT measurements highly depends on the procedures followed during the measurement. Several elements of good practice have been given in the previous sections. Work is going on to document good measuring procedures. In Germany, a good practice guide exists as part of the standard guideline VDI 2630-1.2 [89].

As an example of such guideline, consider e.g. the rotation of the workpiece on the rotary table. A stable mounting of the part is necessary to avoid blurriness due to movement, as is well known from any imaging technique. However, the stable mounting must not be achieved with massive metal fixtures like on tactile CMM machines, as these can disturb the CT measurement due to their own X-ray absorption. Additionally, large fixtures may require to lower the magnification of the measurement leading to worse measurement conditions or may affect the free rotation of the part near the detector (for low magnifications) or near the X-ray tube (for high magnifications). A couple of techniques exist to solve the problem of workpiece fixturing, e.g. use of fixation elements made from carbon fiber, use of low absorbing ribbon canvas or gluing of the workpiece on a mounting rod or plate. One may also use hard foam cuttings, which may contain the negative of the workpiece

geometry for better fixing. It is important that the foam is not too soft to avoid material setting.

8. Applications

CT metrology has some major benefits to other CMM inspection methods (see also Section 1):

- It is today the only method allowing measurement of internal dimensions in a non-destructive way (i.e. without destroying or cutting the component, meaning that the component is still usable after quality control). This is of particular importance for complex cast objects (produced with destroyable cores) or additive manufactured components (e.g. rapid prototyping) that often involve "non-reachable" inner geometries.
- It allows to measure components in the assembled state. This is important as dimensions may differ between non-assembled and assembled components, explaining why assemblies may fail, even if all non-assembled components are within specifications.
- Multi-material components also call for CT metrology, as it is the only method to measure geometry and dimensions at the interface of multi-material components, like for 2 K injection molded products, plastic components with metallic inserts, coated workpieces, etc.
- It allows performing dimensional and material quality assessment within only one quality inspection job. Examples are given in Figs. 33 and 34. Other examples of combined control are reported in [82,83,87].

A first example of a part with inaccessible internal features is the race car oil manifold shown in Fig. 14. It involves many internal holes that require not only measurement of the diameter, but also straightness, position, orientation, etc. Fig. 14b compares the external geometry to the nominal CAD geometry. Fig. 14c is an artificial 2D cut through the manifold allowing inspection of some internal geometrical elements. Real 3D inspection is important in this case, as such manifold contains many intersecting pipes resulting in complex 3D geometries. CT measurement may also be used to detect internal burrs at those intersections that might cause malfunctioning. Fig. 14d represents the external reconstructed geometry with some CT distance measurement between holes.

A second example yielding complex internal geometries is the injection nozzle depicted in Fig. 2d. It illustrates the unique possibility of additive manufacturing (in casu metal selective laser sintering) to build parts with intricate "conformal" cooling channels. The left picture represent the nozzle that was cut through after the CT measurement. It allowed a-posteriori comparison of the CT measurements (right pictures) with other dimensional measurements. The color images in the center compare the geometry of the cooling channels (top) and of the part (bottom) with the CAD file used for additive manufacturing.

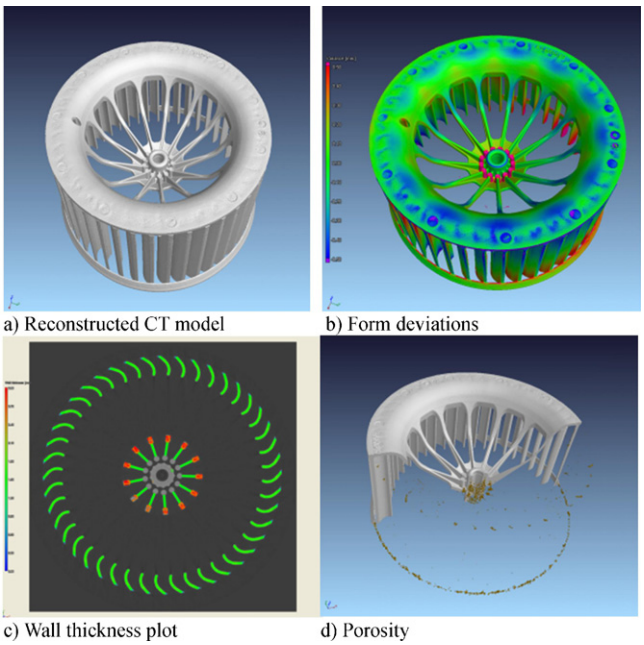

Fig. 33. Car inlet fan: geometric (b and c) and material (d) control.

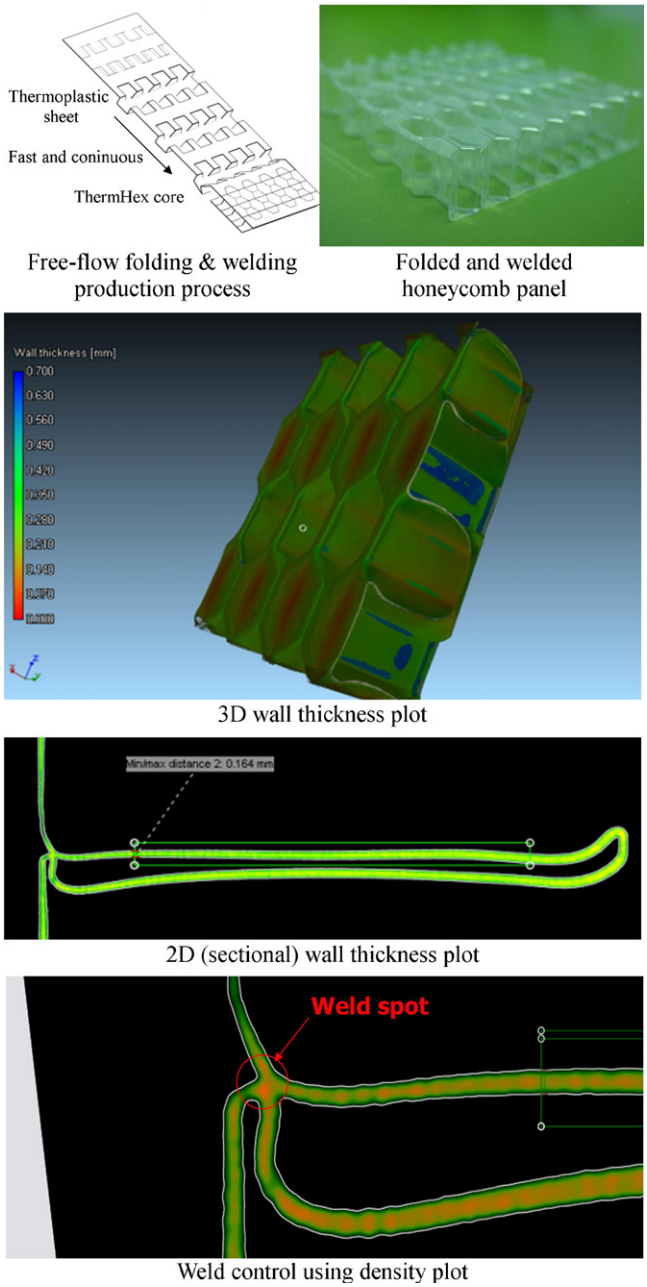

Fig. 34. Application to honeycomb panel.

Fig. 12 is an example of dimensional metrology applied to turbine blades. A lot of geometrical parameters have to be checked, for instance the thickness of inner ribs. Dimensions falling within tolerance are highlighted green, others are highlighted red. Measurements are done at 5 different cross sections of the blade and used to establish a global pass-fail quality inspection report. The same CT data set is also used to check for casting defects in the blades: e.g. inclusions, pores, etc.

Fig. 2a illustrates quality inspection of a lamp bulb involving several materials: glass bulb, metallic electrodes, and ceramic socket. Dimensional parameters that are measured include: alignment of the electrodes and their perpendicularity to the socket base surface (see angle of 91.815°), spacing of electrodes and symmetry towards

glass bulb, etc. The same CT measurement is also used to check for porosity in the ceramic socket and pores in the glass.

Fig. 33 shows CT measurements done on a cast inlet fan of a car [67]. It involves dimensional measurements (size, deviation from nominal geometry and thickness) as well as material quality control (casting porosity).

Fig. 34 shows the quality control of a honeycomb panel produced in a continuous flow sheet embossing, folding and welding process [14]. The CT measurements are used to control dimensions, wall thickness as well as weld quality.

9. Conclusions

This paper has given a state-of-the-art status report on dimensional X-ray CT measurement. Although application of CT measurement for dimensional quality inspection is quite new, the paper demonstrated that:

- CT metrology has a high potential for dimensional quality control of components with internal cavities that are not accessible with other measuring devices. It also allows for a holistic measurement of mechanical components: i.e. full assessment of inner and outer part surface instead of a limited set of points.
- CT is the only inspection process that allows combining dimensional and material quality control.
- A lot remains to be done to enlarge the applicability of dimensional CT measurement to a larger range of part dimensions and workpiece materials, and to ensure measuring accuracy, traceabilty and to assess measurement uncertainty.
- The number of applications and number of installed systems is growing rapidly.
- Full benefit of CT will in future be achieved by the advent of multi-sensor systems applying data fusion techniques.
- CT might substitute other measurement and testing systems (e.g. optical systems) to a certain extent.

Acknowledgments

Co-authorship would have risen to over 15 or more if all contributors would have to be recognized this way. Special thanks go to colleagues and researchers from the labs of the authors that directly contributed to the paper: Dr. U. Neuschaefer-Rube, Dr. H. Bosse, Dr. K. Ehrig, Dr. W. Dewulf, K. Kiekens, F. Welkenhuyzen, Y. Tan, B. Boeckmans, C. Niggemann, N. Van Gestel, Dr. R. Christoph, Dr. Ph. Bleys, and Dr. G. Kerckhofs. Thanks also to the colleagues and board of CIRP STC-P and to the many organizations having sponsored and funded the research activities on CT metrology in the various labs.

References

[1] Ambrose J, Hounsfield G (1973) Computerized Transverse Axial Tomography. *British Journal of Radiology* 46:1023–1047.
[2] Ball J, Moore A (1997) *Essential Physics for Radiographers*. 3rd ed. Blackwell Science, Oxford.
[3] Balsamo A, Di Ciommo M, Mugno R, Sartori S (1996) Towards Instrument-Oriented Calibration of CMMs. *CIRP Annals* 45(1):479.
[4] Bartscher M, et al, (2009) Achieving Traceability of Industrial Computed Tomography. *Proc. 9th Int. Symp. on Measurement and Intelligent Instruments—ISMTII 2009*, D.S. Rozhdestvensky Optical Society, vol. 1 pp. 256–261.
[5] Bartscher M, et al, (2010) Dimensional Control of Technical Components with Computed Tomography. *Metrology and Industry Int. Conf.*
[6] Bartscher M, et al, (2010) *Messung komplexer Geometrien mit industrieller Computertomographie (CT) Applikationen industrieller CT, Normung und Rückführung*. VDI-Bericht 2120. pp. 41–50.
[7] Bartscher M, et al, (2010) Method for a Traceable Geometry Assessment of Arbitrarily Shaped Sculptured Surfaces. *10th Int. Symp. on Measurement and Quality Control ISMQC, Proc.: E3_074_1-4.*
[8] Bartscher M, Hilpert U, Fiedler D (2008) Determination of the Measurement Uncertainty Of Computed Tomography Measurements Using a Cylinder Head as an Example. *Technisches Messen* 75:178–186.
[9] Bartscher M, Hilpert U, Goebbels J, Weidemann G (2007) Enhancement and Proof of Accuracy of Industrial Computed Tomography (CT) Measurements. *CIRP Annals* 56:495–498.
[10] Bartscher M, Hilpert U, Härtig F, Neuschaefer-Rube U, Goebbels J, Staude A (2008) Industrial Computed Tomography, an Emerging Coordinate Measurement Technology with High Potential. *Proc. of NCSL International Workshop and Symposium*.
[11] Bartscher M, Neukamm M, Koch M, Neuschaefer-Rube U, Staude A, Goebbels J, Ehrig K (2010) Performance Assessment of Geometry Measurement with Mirco-CT Using a Dismountable Workpiece-Near Reference Standard. *Proc. Eur. Conf. on NDT (ECNDT 2010)*, Moscow.
[12] Bartscher M, Neuschaefer-Rube U, Staude A, Ehrig K, Goebbels J (2011) Application of an industrial CT reference standard for cast free-form shaped work pieces. *Proc. Int. Symp. on Digital Ind. Radiology and CT, CD-ROM, paper We.4.3*, Berlin, Juni 20–22.
[13] Bartscher M, Neuschaefer-Rube U, Wäldele F (2004) Computed Tomography—A Highly Potential Tool for Industrial Quality Control and Production Near Measurement. *8th Intern. Symp. on Measurement and Quality Control in Production*.
[14] Bratfisch P, Vandepitte D, Pflug J, Verpoest L (2007) Development and Validation of a Continuous Production Concept for Thermoplastic Honeycomb. *Journal of Sandwich Structures & Materials* 9(2):113–122.
[15] Bryan J (1990) International Status of Thermal Error Research. *CIRP Annals* 39(2):645.
[16] Carmignato S (2007) Traceability of dimensional measurements in computed tomography, *Proc. 8th A.I. Te.M. Conf.*, Montecatini, Italy, ISBN/ISSN: 88-7957-264-4.
[17] Carmignato S (2010) Traceability of Dimensional Measurements from CT Scanning. *Conference on "Application of CT scanning in industry", DTU*, Lyngby, Denmark, 8 June 2010.
[18] Carmignato S, Dreossi D, Mancini L, Marinello F, Tromba G, Savio E (2009) Testing of X-ray Microtomography Systems Using a Traceable Geometrical Standard. *Measurement Science and Technology* 20:084021.
[19] Carmignato S, et al, (2004) CT Techniques for Reconstructing 3D Geometrical Models of Complex Parts: An Approach for Traceability Establishment and Uncertainty Evaluation. *IMEKO Int. Symp. and Mediterranean Conference on Measurement*, 387–390.
[20] Carmignato S, Pierobon A (2010) *International Comparison of CT Systems for Dimensional Metrology: The 'CT Audit' Project*. Industrielle Computertomografie, Tagung, FH Wels, Austria.
[21] Carmignato S, Pierobon A, Savio E (2011) First international intercomparison of computed tomography systems for dimensional metrology. *Proc. of 11th Euspen int. conf., Como, Italy, vol. 1*, 84–87.
[22] Carmignato S, Savio E (2011) Metrological Performance Verification of Coordinate Measuring Systems with Optical Distance Sensors. *International Journal of Precision Technology* 2(2/3):153–171. ISSN: 1755-2060.
[23] Carmignato S, Savio E (2011) Traceable Volume Measurements using Coordinate Measuring Systems. *CIRP Annals* 60(1):519–522.
[24] Chantler CT (2000) Detailed Tabulation of Atomic Form Factors, Photoelectric Absorption and Scattering Cross Section, and Mass Attenuation Coefficients in the Vicinity of Absorption Edges in the Soft X-Ray Addressing Convergence Issues of Earlier Work. *Journal of Physical and Chemical Reference Data* 29(4):597–1048.
[25] Christoph R, Rauh W (2007) Measuring Precisely and Traceably Using X-ray Computed Tomography. *Proc. XII. Int. Colloquium on Surfaces*, 346–354.
[26] Christoph R, Schmidt I (2010) Dimensionelle Vielpunktmessung an Mikrostrukturen–Vergleich zwischen CT und taktil-optischer Messung. *Fachtagung Industrielle Computertomografie Zerstörungsfreie Bauteilprüfung, 3D-Materialcharakterisierung und Geometriebestimmung*, Wels, Austria, 27–29 September 2010, 211–217.
[27] De Chiffre L, Hansen HN, Morace RE (2005) Comparison of Coordinate Measuring Machines using an Optomechanical Hole Plate. *CIRP Annals* 54(1):479–482.
[28] Ehrig K, Staude A, Goebbels J, Bartscher M, Koch M, Neukamm M (2010) Evaluierung von Testkörpern zur Strahlaufhärtungskorrektur beim dimensionellen Messen mit Computertomographie. *Proc. of Industrielle Computertomografie*.
[29] Feldkamp LA, Davis LC, Kress JW (1984) Practical Cone-Beam Algorithm. *Journal of the Optical Society of America A* 1:612–619.
[30] Fiedler D, Bartscher M, Hilpert U (2004) Dimensionelle Messabweichungen eine industriellen 2D-Computertomographen: Einfluss der Werkstückrauheit. *DGZfP-Proc. BB 89-CD*.
[31] Franz M (2008) *EAR – Einsatzsynchrone-Artefakt-Reduktion*, PhD thesis, University of Erlangen-Nuremberg.
[32] GE/phoenix (2009) *Prüfbericht, 3D Präzisionsprüfung CT, Prüfbericht zur Bestimmung der Messgenauigkeit von CT-Systemen*, pp. 1–8.
[33] Gondrom S, Schröpfer S (1999) Digital Computed Laminography and Tomosynthesis—Functional Principles and Industrial Applications. *Int. Symp. on Computerized Tomography for Industrial Applications and Image Processing in Radiology, Berlin, Germany, 15–17 March*. (Proc. BB 67-CD published by DGZfP, NDT.net, July 1999 vol. 4 no. 7).
[34] Haitham Shammaa M, Ohtake Y, Suzuki H (2010) Segmentation of Multi-Material CT Data of Mechanical Parts for Extracting Boundary Surfaces. *Computer-Aided Design* 42:118128.
[35] Hanke R, Fuchs T, Uhlmann N (2008) X-ray Based Methods for Non-Destructive Testing and Material Characterization. *Nuclear Instruments and Methods in Physics Research A* 591:14–18.
[36] Hansen HN, De Chiffre L (1997) A Combined Optical and Mechanical Reference Artefact for Coordinate Measuring Machines. *CIRP Annals* 46(1):467.
[37] Härtig F, Krystek M (2009) Correct Treatment of Systematic Errors in the Evaluation of Measurement Uncertainty, D.S. Rozhdestvensky Optical Society. *9th Int. Symp. Measurement and Intelligent Instruments – ISMTII 2009*, Saint-Petersburg, Russia, vol. 1, 16–19.

[38] Heinzl C, Amirkhanov A, Gröller E, Kastner J, Reiter M (2011) Fast Estimation of Optimal Specimen Placements in 3D X-ray Computed Tomography. *Proc. Int. Symp. on Digital Ind. Radiology and CT, CD-ROM, poster P6*, Berlin, Juni 20–22.

[39] Heinzl Ch, Kastner J, Göller E (2007) Surface Extraction from Multi-Material Components for Metrology using Dual Energy CT. *IEEE Transactions on Visualization and Computer Graphics* 13(6):1520–1527.

[40] Hiller J, Kasperl S (2010) Charakterisierung und Modellierung eines μCT-Systems, 15. *ITG/GMA-Fachtagung Sensoren und Messsysteme* 400–405.

[41] Hiller J, Kasperl S, Hilpert U, Bartscher M (2007) Coordinate Measuring with Industrial X-ray Computed Tomography. *Technisches Messen* 74:553–564.

[42] ISO 14253-1 (1998) *GPS—Inspection by Measurement of Workpieces and Measuring Equipment—Part 1: Decision Rules for Proving Conformance or Non-Conformance with Specifications*.

[43] ISO, GUM, JCGM 100 (2008) *Evaluation of Measurement Data–Guide to the Expression of Uncertainty in Measurement*.

[44] ISO, GUM, Suppl. 1, JCGM 101 (2008) *Evaluation of Measurement Data – Supplement 1 to the "Guide to the Expression of Uncertainty in Measurement" – Propagation of Distributions Using a Monte Carlo Method*.

[45] ISO/DTS 15530 (2008) *GPS – CMM: Technique for Determining the Uncertainty of Measurement—Part 1–4*.

[46] Jaenisch G, Bellon C, Ewert U (2008) aRTist—Analytical RT Inspection Simulation Tool for Industrial Application. *17th World Conf. on Nondestructive Testing*.

[47] Jaenisch G, Bellon C, Samadurau U, Zhukovskiy M, Podoliako S (2006) McRay—a Monte Carlo Model Coupled to CAD for Radiation Techniques. *European Conf. NDT, Tu. 4.3.3*.

[48] Kak AC, Slaney M (1988) *Principles of Computerized Tomographic Imaging*. IEEE Press, New York.

[49] Kalender WA (2006) X-ray Computed Tomography. *Physics in Medicine and Biology* 51:R29–43.

[50] Kasperl S, et al, (2002) Reducing Artefacts in Industrial 3D Computed Tomography (CT). *Proc: 8th ECNDT*, Barcelona, Spain.

[51] Kasperl S, Hiller J, Krumm M (2009) Computed Tomography Metrology in Industrial Research and Development. *MP Material Testing* 51:405–411.

[52] Kerckhofs G, Schrooten J, Van Cleynenbreugel T, Lomov SV, Wevers M (2008) Validation of X-ray Micro-CT as an Imaging Tool for Porous Structures. *Review of Scientific Instruments* 79(1):1–9. Article number 013711.

[53] Kerckhofs G, Schrooten J, Wevers M, et al, (2006) Standardisation and Validation of Micro-CT for the Morphological Characterisation of Porous Structures. *Proc. 9th Eur. Conf. Non-Destructive Testing (ECNDT)*, Berlin, Germany, 25–29 September, 1–12.

[54] Kiekens K, Dewulf W, Voet A, Kruth J-P, et al, (2010) A Test Object for Calibration and Accuracy Assessment in X-ray CT metrology. *Proc. IMEKO 10th Int. Symp. on Measurement and Quality Control, B6_86_1-4*.

[55] Knaup M, Stenner Ph, Kachelrieß M (2007) Rawdata-Based Dual Energy CT (DECT) from Inconsistent Scans. *IEEE Nuclear Science Symposium Conference Record*, vol. M26-268, 4457–4459.

[56] Krämer Ph, Weckenmann A (2010) Multi-Energy Image Stack Fusion in Computed Tomography. *Measurement Science & Technology* 21:045105.

[57] Krämer Ph, Weckenmann A (2010) Simulative Abschätzung der Messunsicherheit von Messungen mit Röntgen-Computertomographie. in Kastner J, (Ed.) *Proc. Industr. Computertomografie*243–248. ISBN 978-3-8322-9418-2.

[58] Kruth J-P, et al, (2001) Compensation of Static and Transient Thermal Errors on CMMs. *CIRP Annals* 50(1):p.377–380.

[59] Kruth J-P, Van Gestel N, Bleys P, Welkenhuyzen F (2009) Uncertainty Determination for CMMs by Monte Carlo simulation Integrating Feature Form Deviations. *CIRP Annals* 58(1):463–466.

[60] Lettenbauer H (2010) Metrotomography—Metrology in a New Dimension. *Conf. on Application of CT scanning in industry, DTU*, Lyngby, 8 June 2010.

[61] Lettenbauer H, et al, (2009) Optimized CT Metrology Through Adaptive Image Processing Techniques. *SME—Imaging and Rapid Prototyping Conf.*, Schaumburg, IL.

[62] Meeß R, et al, (2006) Design of a Precision Micro-Assembly Device with 6 DOF. *Proc, 6th Int. Euspen Conf.*, vol. 2, 64–67.

[63] Miceli A, Thierrya R, Flischa A, Sennhausera U, Casalib F, Simoncet M (2007) Monte Carlo Simulations of a High-Resolution X-ray CT System for Industrial Applications. *Nuclear Instruments and Methods in Physics Research A* 583(2–3):313–323.

[64] Mitchell KW (1989) A Generalized Approach to Wall Thickness Measurements in CT Images. *Topical Proc. Industrial Computerized Tomography, ASNT*, 120–124. ISBN 0-931403-89-8.

[65] Nardelli VC, Donatelli GD, Schneider CA, Niggemann C, Schmitt R (2010) Reproducibility of Dimensional Measurements Performed by Computed Tomography. *10th Int. Symp. on Measurement and Quality Control (ISMQC)*, CD-ROM Osaka, Japan.

[66] Neugebauer M, et al, (2007) Ein geometrisches Normal zur Prüfung von Röntgen-Mikro-Computertomografiemesssystemen. *Technisches Messen* 74(11):565–571.

[67] Nikon Metrology/Metris/X-Tek (2011) www.nikonmetrology.com/products/xray_ct_inspection/.

[68] NIST (2011) http://www.nist.gov/pml/data/xraycoef/index.cfm.

[69] Rack A, et al, (2008) High Resolution Synchrotron-Based Radiography and Tomography Using Hard X-rays at the BAM Line (BESSY II). *Nuclear Instruments & Methods in Physics Research A* 586:327–344.

[70] Reimers P, Goebbels J (1983) New Possibilities of Non-Destructive Evaluation by X-ray Computed Tomography. *Materials Evaluation* 41:732–737.

[71] Reisinger S, Kasperl S, Franz M, Hiller J, Schmid U (2011) Simulation-Based Planning of Optimal Conditions for Industrial Computed Tomography. *Proc. Int. Symp. on Digital Ind. Radiology and CT, CD-ROM, poster P6*, Berlin, Juni 20–22.

[72] Reiter M, et al, (2011) Simulation Aided Study for Optimising Industrial X-ray CT Scan Parameters for Non-Destructive Testing and Materials Characterisation. *Proc. Int. Symp. on Digital Ind. Radiology and CT, CD-ROM, poster P6*, Berlin, Juni 20–22.

[73] Rokrok B, et al, (2006) Monte Carlo Simulation of Scattering Phenomenon Effects on Industrial Radiography. *Eur. Conf. on NDT, Tu.4.3.2*.

[74] Sartori S, Zhang GX (1995) Towards Instrument-Oriented Calibration of CMMs. *CIRP Annals* 44(2):599.

[75] Schmidt I, Christoph R (2010) *Dimensionelle Vielpunktmessung an Mikromerkmalen–Computertomografie im Vergleich zu taktil-optischen Sensoren. CT-Tagung*, September 2010, FH-Wels, Oberösterreich.

[76] Schmitt R, Hafner P, Pollmanns S (2008) Artefaktreduzierung in tomographischen Aufnahmen mittels Bilddatenfusion. *Proc. Sensoren und Messsysteme*, 487–495.

[77] Schmitt R, Niggemann C (2010) Einfluss der Bauteilorientierung auf die Messunsicherheit bei dimensionellen Computertomografie. *Proc. Indust. Computertomogr. Conf.*, Wels, Austria, September 2010, 221–226.

[78] Schmitt R, Niggemann C (2010) Uncertainty in Measurement for X-ray-Computed Tomography Using Calibrated Work Pieces. *Measurement Science and Technology* 21(5).

[79] Schulze M, et al, (2010) Der Einfluss unterschiedlicher Materialzusammensetzungen auf das dimensionelle Messen von Mikroobjekten mittels μCT. *Proc. of DGZfP Jahrestagung Erfurt*.

[80] Staude A, Ehrig K, Goebbels J, Bartscher M, Meeß R, Brzoska J, Jung A (2011) private communication.

[81] Staude A, Goebbels J, Ehrig K, Bartscher M, Koch M, Neuschaefer-Rube. (2010) A New Test Piece for Geometry and Defect Measurement with Micro-CT. *Proc. Eur. Conf. on NDT*.

[82] Stephan J, et al, (2010) CT-Qualitätsverbesserungen durch Simulation und Artefaktkorrekturen an Beispielen der Mikromechatronik. *Fraunhofer IPA Workshop F 207*.

[83] Stephan J, Schörner K, Goldamme M (2010) Optimierte Hardwarekomponenten in der CT-Prozesskette zur Steigerung der Performance. *Fraunhofer IPA Workshop F 207: Hochaufgelöste Röntgen-CT-Messtechnik für mikro-mechatronische Systeme*, Stuttgart, 2 July 2010.

[84] Stumbo S, et al, (2004) Direct Analysis of Molybdenum Target Generated X-ray Spectra with a Portable Device. *Medical Physics* 31(10):2763–2770.

[85] Swaelens B, Kruth J-P (1993) Medical Applications of Rapid Prototyping Techniques. *Proc. 4th Intern. Conf. on Rapid Prototyping*, Dayton, 107–120.

[86] Tabary J, Hugonnard P, Mathy F (2007) SINDBAD: A Realistic Multi-Purpose and Scalable X-ray Simulation Tool for NDT Applications. *Int. Symp. on Digital Industrial Radiology and Computed Tomography*, Lyon, France, 25–27 June.

[87] Van Bael S, Kerckhofs G, Moesen M, Pyka G, Kruth J-P, Schrooten J (2009) Morphological and Mechanical Characterization of Ti6Al4V SCAFFOLDS PRODUCED with Selective Laser Melting. *ICTE 2009 Conference*, Portugal, Leira, July 2009.

[88] Van Marcke P, et al, (2006) Optimising X-ray Computer Tomography Images with a CT-Simulator. *2nd Int Workshop on the Application of X-ray CT for Geomaterials* .

[89] VDI/VDE 2630-1.2 (2010) *Computed Tomography in Dimensional Measurement—Influencing Variables on Measurement Results and Recommendations for Computed Tomography Dimensional Measurements*.

[90] VDI/VDE 2630-1.3/VDI/VDE 2617-13 (2009) *Computed Tomography in Dimensional Measurement—Guideline for the Application of DIN EN ISO 10360 for Coordinate Measuring Machines with CT-Sensors*.

[91] VDI/VDE 2630-1.4 (2010) *CT in der dimensionellen Messtechnik—Gegenüberstellung verschiedener dimensioneller Messverfahren*.

[92] Weckenmann A, Jiang X, Sommer K-D, Neuschaefer-Rube U, Seewig J, Shaw L, Estler T (2009) Multisensor Data Fusion in Dimensional Metrology. *CIRP Annals* 58(2):701–721.

[93] Weckenmann A, Krämer P (2009) Anwendung der Computer-Tomographie in der Fertigungsmesstechnik. *Technisches Messen* 76(7–8):340–346.

[94] Weckenmann A, Krämer P (2009) Assessment of Measurement Uncertainty Caused in the Preparation of Measurements Using Computed Tomography. *CD-ROM, Proc. IMEKO XIX World Congress*, 1888–1892. ISBN 978-963-88410-0-1.

[95] Weckenmann A, Krämer P (2009) Computed Tomography for Application in Manufacturing Metrology D. S. Rozhdestvensky Optical Society (Publ.). *Proc. 9th Int. Symp on Measurement and Intelligent Instruments—ISMTII 2009*, vol. 1, 11–26.

[96] Weckenmann A, Krämer P (2009) Predetermination of Measurement Uncertainty in the Application of Computed Tomography. *CD-ROM Proc. 11th CIRP Int. Conf. on Computer Aided Tolerancing (CAT 2009)*, Annecy, France, March 2009, 317–330. ISBN 978-1-84821-276-3.

[97] Wenig P, Kasperl S (2006) Examination of the Measurement Uncertainty on Dimensional Measurements by X-ray Computed Tomography. *ECNDT* .

[98] Werth Messtechnik (2011) www.werth.de/de/unser-angebot/.

[99] Wiacker H (1991) Dimensionsanalyse mit der Computertomografie am Beispiel Turbinenschaufel vermessung. *2. Seminar Computertomografie, DGZfP BB 22*, 86–93.

[100] Wilhelm RG, Hocken R, Schwenke H (2001) Task Specific Uncertainty in Coordinate Measurement. *CIRP Annals* 50(2):553–563.

[101] YXLON (2011) www.yxlon.com/ct_systems.

[102] Zaidi H, et al, (2007) Current Status and New Horizons in Monte Carlo Simulation of X-ray CT Scanners. *Medical & Biological Engineering & Computing* 45(9):809–817.

[103] Zeiss (2007) *Measure and Secure Quality in the Workpiece Interior*, www.zeiss.-com/imt (press release 24 October 2007).